

A Josephson-Anderson relation for drag in classical channel flows with streamwise periodicity: Effects of wall roughness

Samvit Kumar¹ and Gregory L. Eyink¹

Department of Applied Mathematics and Statistics, Johns Hopkins University

(*Electronic mail: skumar67@jh.edu, eyink@jhu.edu)

(Dated: 2 July 2024)

The detailed Josephson-Anderson relation equates instantaneous work by pressure drop over any streamwise segment of a general channel and wall-normal flux of spanwise vorticity spatially integrated over that section. This relation was first derived by Huggins for quantum superfluids, but it holds also for internal flows of classical fluids and for external flows around solid bodies, corresponding there to relations of Burgers, Lighthill, Kambe, Howe and others. All of these prior results employ a background potential Euler flow with the same inflow/outflow as the physical flow, just as in Kelvin’s minimum energy theorem, so that the reference potential incorporates information about flow geometry. We here generalize the detailed Josephson-Anderson relation to streamwise periodic channels appropriate for numerical simulation of classical fluid turbulence. We show that the original Neumann b.c. used by Huggins for the background potential create an unphysical vortex sheet in a periodic channel, so that we substitute instead Dirichlet b.c. We show that the minimum energy theorem still holds and our new Josephson-Anderson relation again equates work by pressure drop instantaneously to integrated flux of spanwise vorticity. The result holds for both Newtonian and non-Newtonian fluids and for general curvilinear walls. We illustrate our new formula with numerical results in a periodic channel flow with a single smooth bump, which reveals how vortex separation from the roughness element creates drag at each time instant. Drag and dissipation are thus related to vorticity structure and dynamics locally in space and time, with important applications to drag-reduction and to explanation of anomalous dissipation at high Reynolds numbers.

I. INTRODUCTION

The modern paradigm^{1,2} for drag and dissipation in the theory of quantum superfluids arose from the work of Josephson³ for superconductors and of Anderson⁴ for neutral superfluids, who both noted a time-average relation between drops of voltage/pressure in flow through wires/channels and the cross-stream flux of quantized magnetic-flux/vortex lines. It was subsequently shown by Huggins⁵ that a “detailed Josephson-Anderson (JA) relation” holds between instantaneous work by pressure drop and integrated flux of vorticity across the mass flux of the background potential associated to the ground-state quantum superflow. These results are the basis of contemporary solutions to the “drag reduction” problem in high-temperature superconductors, where, above some critical current, nucleation and motion of magnetic vortices creates an effective voltage drop and loss of superconductivity. The remedy is to introduce impurities and disorder to pin the vortices and prevent their cross-stream motion, thus restoring dissipationless flow of electric current^{6,7}.

It was noted by Anderson⁴ and by Huggins⁵ that corresponding results hold for classical fluids described by the viscous Navier-Stokes equations. Eyink⁸ pointed out that the time-average result had been invoked already by Taylor⁹ for classical turbulent pipe flow and that an instantaneous relation between pressure gradients and vorticity flux at solid surfaces was derived by Lighthill¹⁰, both anticipating the results for quantum fluids. Subsequently, Eyink¹¹ showed that Huggins’ detailed Josephson-Anderson relation holds also for external flows around solid bodies, relating drag on the body instantaneously to the integrated flux of vorticity across the streamlines of the background potential flow. As reviewed by Biesheuvel and Hagmeijer¹², closely related instantaneous re-

lations for drag in external flows of classical fluids had been previously derived by Burgers, Lighthill and others, especially Howe¹³, and applied to both laminar and turbulent flow regimes. However, to our knowledge there has been no prior study applying the detailed relation of Huggins⁵ to classical channel flows, either laminar or turbulent. Previous work of Huggins¹⁴, Eyink⁸, and Kumar, Meneveau, and Eyink¹⁵ has investigated classical turbulent channel flow using only the time-averaged relation of Taylor⁹ and Anderson⁴, rather than the detailed relation which reveals the instantaneous connection between drag and vorticity dynamics.

We shall show in this paper that the detailed Josephson-Anderson relation in the original form of Huggins⁵ has in fact a significant flaw when applied to classical fluid turbulence. The origin of the problem is Huggins’ assumption that the channel inflow and outflow are pure potential, which is realistic for many superfluid applications where the quantum vortex tangle is strictly confined to some interior section of the channel. However, in applications to classical fluid turbulence this assumption is quite unrealistic as the outflow and very commonly the inflow as well consist of highly rotational flow. Furthermore, we shall see that Huggins’ original derivation, when carried out with the streamwise periodic boundary conditions that are most common in numerical simulations, introduces a spurious vortex sheet into the reference “potential” flow. To avoid these serious difficulties we show here that it suffices to use instead a reference potential which matches only the mean mass flux of the physical flow and not the instantaneous inflow and outflow fields. We show nevertheless that the original derivation of Huggins⁵ goes through with only minor modifications for this new choice of potential and yields again an instantaneous relation between work by pressure drop and spatially integrated vorticity flux. We then present a sample numerical application for turbulent channel

flow with a single smooth bump at modest Reynolds number, but sufficiently high that flow separation is observed with shedding of a rotational wake. In this flow we relate the instantaneous drag arising from both skin friction and pressure forces (form drag) to the vorticity flux from the boundary arising from separation. Our results thus reveal a deep unity to the origin of drag in both classical and quantum fluids.

The results presented here build upon pioneering work of K. R. Sreenivasan, who has made seminal contributions to turbulence in both quantum and classical fluids. In particular, Bewley *et al.*¹⁶ and Fonda, Sreenivasan, and Lathrop^{17,18} developed the first experimental methods to visualize quantized vortices in a superfluid flow and to verify the reconnection dynamics which has been widely theorized to account for superfluid turbulent dissipation, going back to Feynman¹⁹. We shall discuss below the relation of our results with such reconnection processes. In addition, Sreenivasan²⁰ and Sreenivasan and Sahay²¹ have made fundamental contributions to the Reynolds-number scaling of turbulent wall-bounded flows, continuing in more recent works^{22,23}. The persistent viscous effects identified by Sreenivasan and Sahay²¹ make a very important contribution in particular to vorticity flux^{8,15} in wall-bounded flows, which is very relevant to our subject. Finally, the detailed Josephson-Anderson relation has direct applications to problems of polymer drag reduction studied by Sreenivasan and White²⁴ and turbulent energy dissipation rate studied in classic works of Sreenivasan^{25,26}, and Meneveau and Sreenivasan²⁷ which we discuss briefly below. A great legacy of Sreeni's research career is a strong interdisciplinary point of view and a search for general unifying principles, an example which we strive to emulate in this contribution to the Special Issue in honor of his 75th birthday.

II. PRIOR WORK OF HUGGINS AND OTHERS

In this section we very briefly review the detailed relation of Huggins, its derivation, and the closely related results obtained by others for external flows. Huggins⁵ considered a classical incompressible fluid at constant mass density ρ and with kinematic viscosity ν subject to accelerations both from a conservative force $-\nabla Q$ and from a non-conservative force $-\mathbf{f}$ satisfying $\nabla \times \mathbf{f} \neq \mathbf{0}$, described by the incompressible Navier-Stokes equation written as

$$\partial_t \mathbf{u} = \mathbf{u} \times \boldsymbol{\omega} - \nu \nabla \times \boldsymbol{\omega} - \nabla(p + |\mathbf{u}|^2/2 + Q) - \mathbf{f}. \quad (1)$$

A fundamental step made by Huggins^{14,28} was to rewrite the above momentum balance in the form

$$\partial_t u_i = (1/2)\epsilon_{ijk}\Sigma_{jk} - \partial_i h, \quad (2)$$

with anti-symmetric *vorticity flux tensor*

$$\Sigma_{ij} = u_i \omega_j - u_j \omega_i - \nu(\partial_i \omega_j - \partial_j \omega_i) - \epsilon_{ijk} f_k, \quad (3)$$

from vorticity advection, stretching, viscous diffusion and Magnus effect of the body force, and *total pressure*

$$h = p + |\mathbf{u}|^2/2 + Q. \quad (4)$$

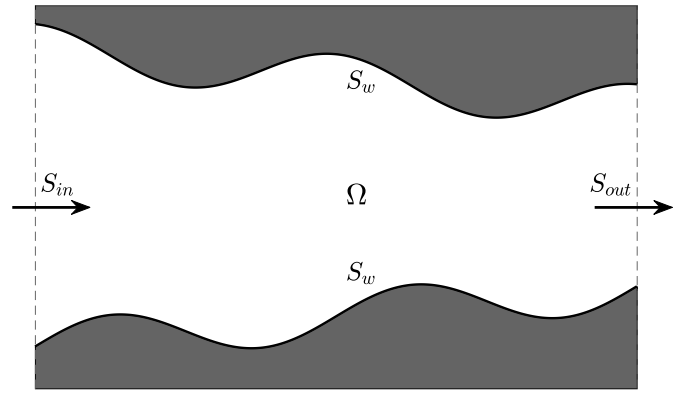


FIG. 1: Context of the detailed relation of Huggins⁵: Flow through a channel Ω with inflow surface S_{in} , outflow surface S_{out} , and sidewalls S_w .

including both the hydrostatic and the dynamic pressures. The tensor Σ_{ij} represents the flux of the j th vorticity component in the i th coordinate direction. The latter interpretation is made clear by taking the curl of the momentum equation (1), which yields a local conservation law for vector vorticity:

$$\partial_t \boldsymbol{\omega}_j + \partial_i \Sigma_{ij} = 0. \quad (5)$$

The equation (2) thus shows directly the connection between momentum balance and vorticity transport, and this equation is itself the most elementary version of the classical Josephson-Anderson relation.

To derive his detailed relation, Huggins⁵ considered very general flows through pipes and channels, whose walls might be curved or bent, with rough or wavy surfaces, and with variable cross-sections. For example, a flow through an orifice in a wall is a classical application of the JA-relation in superfluids. See Figure 1 for the general situation. Huggins assumed given velocity at the inflow surface S_{in} and at the outflow surface S_{out} and stick boundary conditions at the sidewall S_w :

$$\mathbf{u}|_{S_{in}} = \mathbf{u}_{in}, \quad \mathbf{u}|_{S_{out}} = \mathbf{u}_{out}, \quad \mathbf{u}|_{S_w} = \mathbf{0}. \quad (6)$$

A key idea of Huggins⁵ was then to compare the viscous rotational flow solving the incompressible Navier-Stokes equation (1) with an ideal incompressible potential flow $\mathbf{u}_\phi = \nabla \phi$ solving the Euler equations with the same in-flow and out-flow:

$$\begin{aligned} \mathbf{n} \cdot \mathbf{u}_\phi|_{S_{in}} &= \mathbf{n} \cdot \mathbf{u}_{in}, & \mathbf{n} \cdot \mathbf{u}_\phi|_{S_{out}} &= \mathbf{n} \cdot \mathbf{u}_{out}, \\ \mathbf{n} \cdot \mathbf{u}_\phi|_{S_w} &= 0. \end{aligned} \quad (7)$$

where \mathbf{n} is the unit normal at the boundary pointing into the fluid interior. In superfluid applications this potential flow corresponds to the dissipation-less flow in the quantum ground state in the absence of any quantized vortex excitations. This is in fact the flow with the least energy among all incompressible flows with the boundary conditions (7) according to the Kelvin minimum energy theorem²⁹⁻³²; see also below. The scalar potential ϕ solves the Laplace equation $\nabla^2 \phi = 0$ in the open flow domain Ω with Neumann boundary conditions supplied by (7) and is thus unique up to a spatial constant. In that

case, the Euler dynamics reduce to the Bernoulli equation

$$\partial_t \phi + \frac{1}{2} |\mathbf{u}_\phi|^2 + p_\phi + Q = c(t), \quad (8)$$

for a spatial constant $c(t)$, which yields the static Euler pressure p_ϕ and the total Euler pressure $h_\phi = p_\phi + |\mathbf{u}_\phi|^2/2 + Q$ given the velocity potential ϕ . It is a direct consequence of (8) that the potential Euler solution experiences no mean drag, since long-time averaging denoted by $\langle \cdot \rangle$ yields the relation

$$\langle \nabla h_\phi \rangle = \mathbf{0} \quad (9)$$

and thus mass flux occurs without any mean gradient of the total pressure. Likewise, in terms of the kinetic energy of the potential flow

$$E_\phi = (\rho/2) \int_\Omega |\mathbf{u}_\phi|^2 dV, \quad (10)$$

one finds using the Bernoulli equation (8) that

$$\begin{aligned} \frac{dE_\phi}{dt} &= \rho \int_\Omega \mathbf{u}_\phi \cdot \nabla (\partial_t \phi) dV = -\rho \int_{\partial\Omega} (\partial_t \phi) \mathbf{u}_\phi \cdot \mathbf{n} dA \\ &= \int_{S_{in}} h_\phi dJ - \int_{S_{out}} h_\phi dJ := \mathcal{W}_\phi, \end{aligned} \quad (11)$$

where $dJ = \rho \mathbf{u}_\phi \cdot d\mathbf{A}$ is the mass flux element along the potential flow and where the last line defines the instantaneous rate of work \mathcal{W}_ϕ done by the potential pressure h_ϕ . As long as the inflow/outflow conditions remain bounded in time, then also E_ϕ remains bounded and long-time averaging yields

$$\langle \mathcal{W}_\phi \rangle = 0. \quad (12)$$

The relations (9),(12) may be regarded as analogues of the ‘‘d’Alembert paradox’’^{33,34} for potential fluid flows through pipes and channels.

The detailed relation of Huggins⁵ connected vortex motion further to energy balance. It was natural in Huggins’ analysis to adopt as reference the potential flow $\mathbf{u}_\phi = \nabla \phi$ which represents the superfluid velocity in the quantum ground state. Huggins thus decomposed the rate of work by the total pressure head

$$\mathcal{W} = \int_{S_{in}} h dJ - \int_{S_{out}} h dJ \quad (13)$$

as $\mathcal{W} = \mathcal{W}_\phi + \mathcal{W}_\omega$, where

$$\mathcal{W}_\omega = \int_{S_{in}} h_\omega dJ - \int_{S_{out}} h_\omega dJ. \quad (14)$$

is the rate of work done by the head of *total rotational pressure* $h_\omega = h - h_\phi$. Because of (12), \mathcal{W}_ω represents the ‘‘effective work’’ which solely contributes to the long-time average. The main result of Huggins states that \mathcal{W}_ω is exactly equal to another quantity \mathcal{T} that measures the flux of vorticity across the mass current of the background potential, given by the following equivalent expressions

$$\begin{aligned} \mathcal{T} &= - \int_\Omega \rho \mathbf{u}_\phi \cdot (\mathbf{u} \times \boldsymbol{\omega} - \nu \nabla \times \boldsymbol{\omega} - \mathbf{f}) dV \\ &= - \int dJ \int (\mathbf{u} \times \boldsymbol{\omega} - \nu \nabla \times \boldsymbol{\omega} - \mathbf{f}) \cdot d\boldsymbol{\ell} \\ &= - \frac{1}{2} \int dJ \int \varepsilon_{ijk} \Sigma_{ij} d\ell_k, \end{aligned} \quad (15)$$

where the line integrals are along streamlines of the potential flow. In fact, we shall see that \mathcal{T} represents a transfer of kinetic energy from potential to rotational motions. The *detailed Josephson-Anderson relation* of Huggins⁵ then states precisely the identity

$$\mathcal{W}_\omega = \mathcal{T}. \quad (16)$$

In other words, the effective rate of work done by the rotational pressure head is instantaneously related to the transverse motion of vortex lines across the potential flow. This relation is useful precisely because \mathcal{W}_ω is the work contribution which is hard to understand and to compute, whereas \mathcal{W}_ϕ has transparent meaning and ϕ is computable at each time instant by standard solvers for the Laplace equation.

Because we must generalize this result for classical turbulent channel flow, it is useful to reprise here the short proof. Huggins⁵ obtained (16) by deriving a complementary equation for the rotational fluid motions and by then considering the coupled energy balances for potential and rotational flows. The rotational velocity field defined by Huggins was $\mathbf{u}_\omega := \mathbf{u} - \mathbf{u}_\phi$, which accounts for all vorticity in the flow. Its governing equations are easily obtained by subtracting the Euler equation for \mathbf{u}_ϕ from the Navier-Stokes (1), yielding,

$$\partial_t \mathbf{u}_\omega = \mathbf{u} \times \boldsymbol{\omega} - \nu \nabla \times \boldsymbol{\omega} - \nabla h_\omega \quad (17)$$

where h_ω can be rewritten (up to a spatial constant) as

$$h_\omega = h + \partial_t \phi = p_\omega / \rho + |\mathbf{u}_\omega|^2 / 2 + \mathbf{u}_\omega \cdot \mathbf{u}_\phi. \quad (18)$$

with $p_\omega = p - p_\phi$ and \mathbf{u}_ω satisfies the boundary conditions

$$\begin{aligned} \mathbf{u}_\omega|_{S_{in}} &= (\mathbf{u} - \mathbf{u}_\phi)|_{S_{in}}, & \mathbf{u}_\omega|_{S_{out}} &= (\mathbf{u} - \mathbf{u}_\phi)|_{S_{out}}, \\ \mathbf{u}_\omega|_{S_w} &= -\mathbf{u}_\phi|_{S_w}. \end{aligned} \quad (19)$$

In particular,

$$\mathbf{n} \cdot \mathbf{u}_\omega|_{S_{in}} = \mathbf{n} \cdot \mathbf{u}_\omega|_{S_{out}} = \mathbf{n} \cdot \mathbf{u}_\omega|_{S_w} = 0. \quad (20)$$

The latter render the potential velocity \mathbf{u}_ϕ and the rotational velocity \mathbf{u}_ω orthogonal, since their spatial L^2 inner product is

$$\int_\Omega \mathbf{u}_\phi \cdot \mathbf{u}_\omega dV = \int_\Omega \nabla \cdot (\phi \mathbf{u}_\omega) dV = - \int_{\partial\Omega} \phi \mathbf{u}_\omega \cdot \mathbf{n} dS = 0. \quad (21)$$

This orthogonality is the essence of Kelvin’s minimum energy theorem, since it implies that the total kinetic energy $E = (\rho/2) \int_\Omega |\mathbf{u}|^2 dV$ in the channel is a sum of potential and rotational contributions, $E = E_\phi + E_\omega$, with the kinetic energy of rotational motions given by

$$E_\omega = (\rho/2) \int_\Omega |\mathbf{u}_\omega|^2 dV.$$

In that case, the minimum kinetic energy E for all incompressible velocity fields \mathbf{u} satisfying the b.c. (7) is obviously achieved with $\mathbf{u}_\omega = \mathbf{0}$ or $\mathbf{u} = \mathbf{u}_\phi$.

From the above equations, Huggins⁵ derived balance equations for E_ω and E_ϕ . Taking the dot product of (17) with $\rho\mathbf{u}_\omega$ and integrating over the channel volume yields

$$\frac{dE_\omega}{dt} = \mathcal{T} - \mathcal{D} + \int_{S_{in}} h_\omega \mathbf{u}_\omega \cdot \mathbf{n} dA + \int_{S_{out}} h_\omega \mathbf{u}_\omega \cdot \mathbf{n} dA, \quad (22)$$

so that the b.c. (20) give the final equation for E_ω as

$$\frac{dE_\omega}{dt} = \mathcal{T} - \mathcal{D} \quad (23)$$

where \mathcal{T} is given by (15) and the total energy dissipation by non-conservative forces is given by

$$\mathcal{D} = \int_{\Omega} (\eta |\boldsymbol{\omega}|^2 + \rho \mathbf{u} \cdot \mathbf{f}) dV.$$

with $\eta = \nu\rho$ the shear viscosity. The total energy satisfies of course the standard balance

$$\frac{dE}{dt} = \mathcal{W} - \mathcal{D}. \quad (24)$$

The equation for E_ϕ is then obtained simply by subtracting the equations (24) and (23), yielding,

$$\frac{dE_\phi}{dt} = \mathcal{W} - \mathcal{T}. \quad (25)$$

The two balance equations (23),(25) show that the work \mathcal{W} done by the pressure head goes entirely into potential flow energy, which is in turn transferred by vortex motion through the term \mathcal{T} into rotational flow energy, and then ultimately disposed by the dissipation \mathcal{D} due to viscosity and other non-ideal forces acting on the rotational flow. As a final step, Huggins⁵ then substituted the relation (11) for dE_ϕ/dt into (25) which, recalling the definition $\mathcal{W}_\omega := \mathcal{W} - \mathcal{W}_\phi$, yields directly the detailed Josephson-Anderson relation (16).

The previous results are very closely analogous to well-known results for external flows around bodies in translational motion with velocity $-\mathbf{V}(t)$ or equivalently, by a change of reference frame, flows around bodies at rest with fluid velocity $\mathbf{V}(t)$ at infinity. We prefer to state the results in the latter body frame and we omit all proofs, referring to standard sources such as Batchelor³¹, Lighthill³⁵, Wu³⁶, Eyink¹¹ and the review of Biesheuvel and Hagmeijer¹². The main object of interest here is the force acting on the fixed body B

$$\mathbf{F}(t) = \int_{\partial B} (-P\mathbf{n} + \rho\boldsymbol{\tau}_w) dA$$

with $P = \rho p$ the thermodynamic pressure and with $\boldsymbol{\tau}_w = \nu\boldsymbol{\omega} \times \mathbf{n} = 2\nu\mathbf{S} \cdot \mathbf{n}$ the viscous skin friction. This force is of course related to fluid impulse $\mathbf{I}(t)$ by the well-known relation $\mathbf{F}(t) = -d\mathbf{I}/dt$. In the special case of potential flow satisfying

the no-penetration b.c. $\partial\phi/\partial n = 0$ at the body surface ∂B , the force is given by

$$\mathbf{F}_\phi(t) = - \int_{\partial B} P_\phi \mathbf{n} dA$$

and the impulse by

$$\mathbf{I}_\phi(t) = -\rho \int_{\partial B} \phi \mathbf{n} dA$$

once again related by $\mathbf{F}_\phi(t) = -d\mathbf{I}_\phi/dt$. Thus,

$$\langle \mathbf{F}_\phi \rangle = 0$$

which is the ‘‘generalized d’Alembert paradox’’ for bodies in non-uniform translational motion. As in the work of Huggins, Lighthill^{35,37} and others^{11,12} have proposed to divide the flow into the background potential flow fields \mathbf{u}_ϕ , p_ϕ and the complementary rotational fields $\mathbf{u}_\omega = \mathbf{u} - \mathbf{u}_\phi$, $p_\omega = p - p_\phi$. The ‘‘effective force’’ imposed by rotational fluid motions is then

$$\mathbf{F}_\omega(t) = \int_{\partial B} (-P_\omega \mathbf{n} + \rho\boldsymbol{\tau}_w) dA$$

and the impulse of the rotational flow is

$$\mathbf{I}_\omega(t) = \frac{1}{2} \left[\int_{\Omega} \mathbf{x} \times \boldsymbol{\omega}(\mathbf{x}, t) dV + \int_{\partial B} \mathbf{x} \times (\mathbf{n} \times \mathbf{u}_\omega(\mathbf{x}, t)) dA \right]$$

so that $\mathbf{F}_\omega(t) = -d\mathbf{I}_\omega/dt$. Note that $\boldsymbol{\Gamma} = \mathbf{n} \times \mathbf{u}_\phi$ can be regarded as the strength vector of a surface vortex sheet of the potential flow \mathbf{u}_ϕ and since $\mathbf{n} \times \mathbf{u}_\omega = -\mathbf{n} \times \mathbf{u}_\phi$ on ∂B

$$\mathbf{I}_\omega(t) = \frac{1}{2} \int_{\Omega} \mathbf{x} \times \boldsymbol{\omega}_a(\mathbf{x}, t) dV$$

where $\boldsymbol{\omega}_a$ is the so-called *additional vorticity*, with the surface vortex sheet removed. Note that generally $\langle \mathbf{F}_\omega(t) \rangle \neq \mathbf{0}$ because $\mathbf{I}_\omega(t)$ increases monotonically as the rotational wake grows in extent and its impulse is not bounded in time.

In the present context of external flow, the quantity analogous to the rate of pressure work (13) for channel flows is the power dissipated by the drag force:

$$\mathcal{W} := \mathbf{F}(t) \cdot \mathbf{V}(t). \quad (26)$$

The force decomposition $\mathbf{F}(t) = \mathbf{F}_\phi(t) + \mathbf{F}_\omega(t)$ immediately implies a corresponding decomposition of the dissipated power $\mathcal{W}(t) = \mathcal{W}_\phi(t) + \mathcal{W}_\omega(t)$. However, since impulse $\mathbf{I}_\phi(t) = \mathbb{A} \cdot \mathbf{V}(t)$ with \mathbb{A} a time-independent *added mass* tensor depending only on the shape of the body, it follows that $\mathcal{W}_\phi = \mathbf{F}_\phi(t) \cdot \mathbf{V}(t) = \frac{d}{dt} (\frac{1}{2} \mathbf{V}(t) \cdot \mathbb{A} \cdot \mathbf{V}(t))$ and thus

$$\langle \mathcal{W}_\phi \rangle = 0.$$

Just as before, there is no time-average power dissipated by the potential drag force and all of the ‘‘effective dissipation’’ arises from drag force due to rotational flow:

$$\mathcal{W}_\omega := \mathbf{F}_\omega(t) \cdot \mathbf{V}(t) \quad (27)$$

It was shown by Eyink¹¹ that a detailed Josephson-Anderson relation holds for the latter, of the same form as (16):

$$\mathcal{W}_\omega = \mathcal{T}$$

where \mathcal{T} is given by exactly the same expression (15). Thus, power dissipated by drag on the body due to rotational fluid motions is given instantaneously by the space integral of the vorticity flux across the flowlines of the background potential. In fact, this result is just a special case of a more general result of Howe¹³ which applies to arbitrary rigid body motion (translation and rotation) and which gives all force components, not only drag but also lateral forces such as lift.

It was pointed out by Eyink¹¹ that the JA-relation should hold even in the limit of infinite Reynolds number, if spatial integration-by-parts is performed to rewrite the transfer term in (15) instead as

$$\mathcal{T} = -\rho \int_{\Omega} \nabla \mathbf{u}_\phi : \mathbf{u}_\omega \mathbf{u}_\omega dV + \rho \int_{\Omega} \mathbf{u}_\phi \cdot \mathbf{f} dV + \rho \int_{\partial\Omega} \mathbf{u}_\phi \cdot \boldsymbol{\tau}_w dA. \quad (28)$$

This mathematical conjecture of an infinite- Re limit has been verified by Quan and Eyink³⁸ for the case of no body-force ($\mathbf{f} = \mathbf{0}$) in flow around a solid body, providing a new resolution of the famous paradox of d'Alembert^{33,34} and connecting with the Onsager theory of "ideal turbulence"³⁹⁻⁴¹. To derive these conclusions for the limit $Re \rightarrow \infty$ it is crucial that the reference potential flow velocity must be infinitely differentiable or C^∞ , which could indeed be proved for external flow as long as the body surface is correspondingly smooth.

III. A NEW DETAILED RELATION FOR STREAMWISE PERIODIC POISEUILLE FLOWS

The previous developments reviewed above suggest that vorticity flux accounts for wall drag with great generality, in many incompressible fluid flows of practical and theoretical interest, and that the JA relation can provide a novel vorticity-based perspective on drag reduction. Unfortunately, a difficulty occurs in the straightforward application of the original relation of Huggins⁵ to classical turbulent flows through pipes and channels. In that case, the fields \mathbf{u}_{in} and \mathbf{u}_{out} that appear in the boundary conditions (7) for the reference potential flow are both x -slices of a very complex and rough turbulent velocity field. This means that \mathbf{u}_ϕ is generally also spatially complex and rough, inheriting those properties from its boundary conditions. This poses a serious problem for mathematical analysis of the infinite-Reynolds limit³⁸, since the arguments involved depend crucially on the smoothness of the potential flow. Furthermore, this non-smoothness of \mathbf{u}_{in} and \mathbf{u}_{out} makes more demanding the numerical computation of \mathbf{u}_ϕ . The corresponding problem does not appear in typical superfluid applications, since the vortex tangles in that case are generally confined well within the channel interior.

Another important issue is that numerical simulations of turbulent pipe and channel flows in classical fluids very frequently employ periodic boundary conditions in the streamwise direction as a computational convenience. The flow may

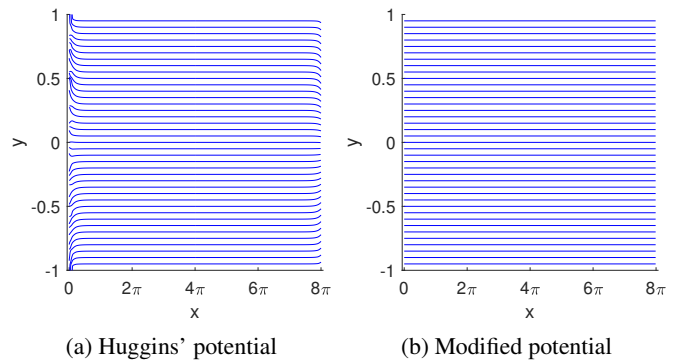


FIG. 2: Streamlines of the reference potential for a snapshot of streamwise-periodic turbulent channel flow

be driven either with a fixed bulk velocity or as Poiseuille flow with a fixed pressure gradient. In the latter case, a standard choice is to use a non-periodic linear potential $Q_{nper} = -\gamma(t)x$, where x is taken as the streamwise direction and $\gamma(t)$ is the resultant streamwise gradient in the total pressure h , but with velocity \mathbf{u} and static pressure p both periodic. This situation is of the type considered by Huggins⁵ but with the ends of the channel periodically joined so that $S_{in} = S_{out}$. In this setting, the naive approach would be to mimic exactly the original derivation and take as reference field the Euler flow with potential ϕ solving Laplace's equation with Neumann boundary conditions (7), without regard for the fact that $\mathbf{u}_{in} = \mathbf{u}_{out}$. All of the analysis and results of Huggins⁵ then carries over in this setting. However, there is a serious difficulty. The potential ϕ is uniquely specified (up to a spatial constant) by the Laplace problem with Neumann boundary conditions (7) and these conditions guarantee that $\mathbf{n} \cdot \mathbf{u}_{\phi,in} = \mathbf{n} \cdot \mathbf{u}_{\phi,out}$ so that $\mathbf{n} \cdot \mathbf{u}$ is x -periodic. However, in general the components of \mathbf{u}_ϕ perpendicular to \mathbf{n} need not be periodic. In fact, any such discontinuity corresponds to a vortex sheet in \mathbf{u}_ϕ at $S_{in} = S_{out}$ with strength $\boldsymbol{\Gamma} = \mathbf{n} \times (\mathbf{u}_{\phi,out} - \mathbf{u}_{\phi,in})$. Since the surface $S_{in} = S_{out}$ was arbitrarily chosen and any x -cross-section could be equally selected for the construction, this means that there is a vortex sheet in the interior of the periodic domain and \mathbf{u}_ϕ is not truly potential.

Both of these problems can be illustrated in the case of turbulent Poiseuille flow through a smooth plane-parallel channel, using data from the Johns Hopkins turbulence database (JHTDB)^{42,43} which hosts data from a numerical simulation at $Re_\tau = 1000$ on a space domain $[0, 8\pi] \times [-1, 1] \times [0, 3\pi]$ with periodic b.c. in the streamwise x -direction and spanwise z -direction, but stick b.c. in the wall-normal y -direction. We have obtained Huggins' reference potential ϕ by solving numerically Laplace's equation with boundary conditions (7), using a 2nd-order central-difference scheme. The streamlines of this potential for one time snapshot from the database are plotted in panel (a) of Fig. 2 and show spatially irregular behavior near in-flow at $x = 0$ and out-flow at $x = 8\pi$. The same irregularity is observed in the results for the wall-normal velocity component v_ϕ plotted in Fig. 3 at in-flow and out-flow. Even more seriously, this velocity component can be seen to be streamwise anti-periodic as is also the spanwise component

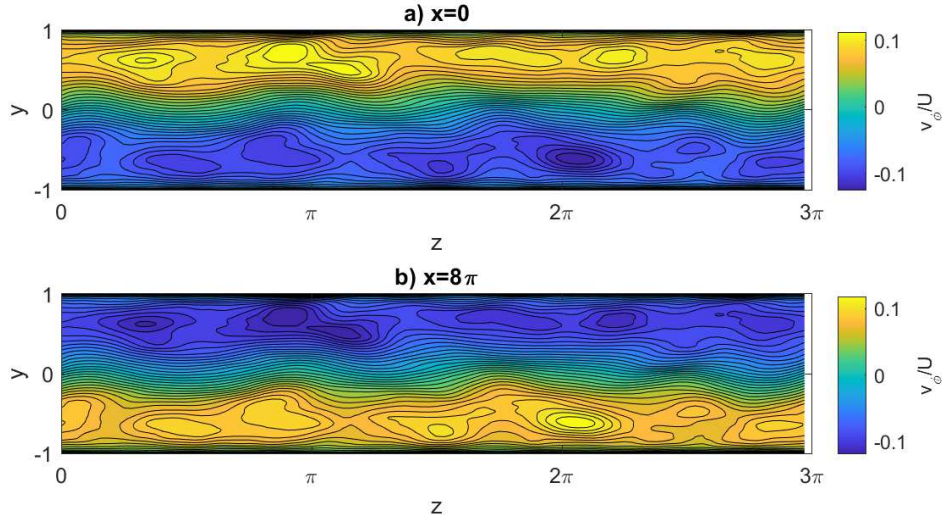


FIG. 3: Anti-periodic wall-normal component of Huggins' potential flow velocity for a snapshot of turbulent channel flow, at inflow $x = 0$ and outflow $x = 8\pi$.

w_ϕ (see Supplementary Materials, §I), both corresponding to a vortex sheet in \mathbf{u}_ϕ . Interestingly, however, after inertial adjustment over a length of order the channel half-width, the potential flow field closely resembles a plug flow with spatially constant velocity $\mathbf{u}_\phi = U\hat{\mathbf{x}}$, for U the bulk flow velocity. The latter observation suggests that it might be possible in this case to use as reference flow the simple Euler solution $\mathbf{u}_\phi = U\hat{\mathbf{x}}$ with non-periodic potential $\phi = Ux$ which has constant values $\phi = 0$ at $x = 0$ and $\phi = 8\pi U$ at $x = 8\pi$. This idea is readily verified.

Motivated by this example, however, we show here that one may more generally derive a Josephson-Anderson relation for streamwise-periodic Poiseuille flows using a potential ϕ satisfying Dirichlet b.c. at the end sections and which is periodic plus a linear part. We can consider generalized pipe and channel flows with curved or rippled walls, but, for technical reasons explained below, we must assume that the flow domain extends over $x \in [-0.5L_x, 0.5L_x]$ and S_{in}, S_{out} are flat surfaces of constant x -value. For the case of channels we assume likewise a spanwise extent $z \in [-0.5L_z, 0.5L_z]$, with periodic b.c. Finally, the flow is assumed driven by a non-periodic potential $Q_{nper} = -\gamma(t)x$, with fluid velocity \mathbf{u} and static pressure p that are x -periodic. As we shall see, with these assumptions alone we may derive a version of the Kelvin minimum energy theorem. However, to derive the JA-relation and to guarantee that the potential flow velocity \mathbf{u}_ϕ is C^∞ on the torus we must require further that the flow domain is reflection-symmetric about the spanwise-wall normal midplane at $x = 0$, as shown in Fig. 4⁴⁴. Additionally, at the intersection of the sidewalls S_w with inflow surface S_{in} and outflow surface S_{out} we assume that the normal vectors satisfy the geometric conditions

$$\mathbf{n}_w \cdot \mathbf{n}_{in} = \mathbf{n}_w \cdot \mathbf{n}_{out} = 0. \quad (29)$$

required for compatibility between Neumann conditions on S_w and Dirichlet conditions on S_{in} and S_{out} .

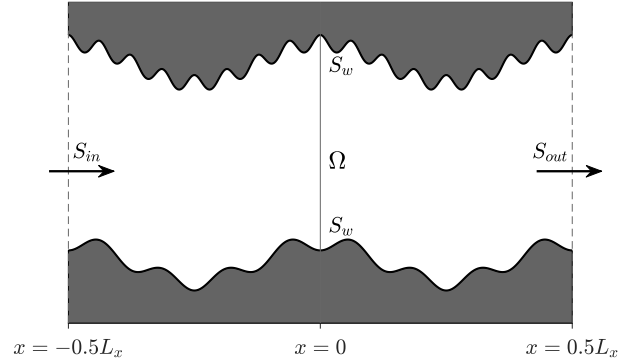


FIG. 4: Flow through a channel Ω with inflow surface S_{in} , outflow surface S_{out} , and sidewalls S_w . The domain is symmetric about the spanwise-wall normal plane at $x=0$.

Under these assumptions we define the potential ϕ of the reference Euler solution to satisfy the Laplace equation, $\nabla^2 \phi = 0$, with mixed Neumann-Dirichlet boundary conditions

$$\left. \frac{\partial \phi}{\partial n} \right|_{S_w} = 0, \quad \phi \Big|_{S_{in}} = -\frac{1}{2}\Phi(t), \quad \phi \Big|_{S_{out}} = +\frac{1}{2}\Phi(t). \quad (30)$$

For channel flow, we assume spanwise periodic boundary conditions as well. Here, the potential difference $\Phi(t)$ is chosen

so that the Euler flow carries the entire mass flux, that is,

$$J_\phi(t) := \rho \int_{S_{in}} \mathbf{u}_\phi \cdot \hat{\mathbf{n}} dA = \rho \int_{S_{out}} \mathbf{u}_\phi \cdot \mathbf{n} dA \quad (31)$$

$$= \rho \int_{S_{in}} \mathbf{u} \cdot \hat{\mathbf{n}} dA = \rho \int_{S_{out}} \mathbf{u} \cdot \mathbf{n} dA := J(t). \quad (32)$$

This potential is easily calculated by exploiting the homogeneity of the problem and first solving for $\phi_* = \phi/\Phi$, which satisfies the Laplace equation, $\nabla^2 \phi_* = 0$ with mixed boundary conditions

$$\frac{\partial \phi_*}{\partial n} \Big|_{S_w} = 0, \quad \phi_* \Big|_{S_{in}} = -\frac{1}{2}, \quad \phi_* \Big|_{S_{out}} = +\frac{1}{2}. \quad (33)$$

for which a unique solution exists. Now, let $\mathbf{u}_{\phi_*} = \nabla \phi_*$ and $J_* = \rho \int_{S_{in}} \mathbf{u}_{\phi_*} \cdot \mathbf{n} dA$, leading to $J(t) = J_* \Phi(t)$ and

$$\phi = \Phi(t) \phi_* = J(t) \phi_* / J_*. \quad (34)$$

Observe that ϕ_* and consequently J_* depend only on the channel geometry. The potential $\phi(t)$ that results for given $J(t)$ is uniquely defined, although in general it may depend upon the arbitrary choice of the surface $S_{in} = S_{out}$ in the periodic domain Ω . We remark in passing also that $E_\phi = (1/2)J\Phi$, as shown by using as curvilinear coordinates the potential ϕ itself and any convenient parameterization of ϕ -isosurfaces and by noting that $d\phi = |\mathbf{u}_\phi| d\ell$ for arclength ℓ along streamlines.

The above construction yields a reference Euler solution \mathbf{u}_ϕ which is C^∞ and x -periodic, when reflection symmetry of Ω about its midplane is assumed. Since $\hat{\phi}(x, y, z) := -\phi(-x, y, z)$ is another solution of the mixed boundary-value problem (30), uniqueness of that solution implies the symmetry property

$$\phi(-x, y, z) = -\phi(x, y, z). \quad (35)$$

This fact will be exploited together with the fact that the harmonic function $\phi \in C^\infty(\hat{\Omega})$ where $\hat{\Omega} = \Omega \setminus (S_{in} \cap S_{out} \cap S_w)$ is the interior of the domain. See Evans⁴⁵, Theorem 2.6, p.28. Note that ϕ will in general be smooth up to S_w if the side-wall S_w is smooth, but we must show that all derivatives approaching $S_{in} = S_{out}$ from both sides agree. It is an elementary consequence of (35) that

$$\partial_x^m \phi(-\frac{L_x}{2}, y, z) = \partial_x^m \phi(+\frac{L_x}{2}, y, z), \quad \text{for all odd } m. \quad (36)$$

We next show by induction that

$$\partial_x^m \phi(-\frac{L_x}{2}, y, z) = \partial_x^m \phi(+\frac{L_x}{2}, y, z) = 0, \quad \text{for all even } m \geq 2. \quad (37)$$

For $m = 2$ this follows by using the fact that ϕ is harmonic and is a spatial constant $\phi = \pm\Phi/2$ for $x = \pm L_x/2$, so that

$$\partial_x^2 \phi(\pm \frac{L_x}{2}, y, z) = -(\partial_y^2 + \partial_z^2) \phi(\pm \frac{L_x}{2}, y, z) = 0.$$

We now assume that (37) holds for all even integers up to m and then note that

$$\partial_x^{m+2} \phi(\pm \frac{L_x}{2}, y, z) = -\partial_x^m (\partial_y^2 + \partial_z^2) \phi(\pm \frac{L_x}{2}, y, z) = 0$$

by using the Laplace equation and the induction hypothesis, thereby completing the induction. It follows from (36),(37) that $\mathbf{u}_\phi = \nabla \phi$ is both x -periodic and C^∞ in Ω .

Note that the velocity potential ϕ itself obviously cannot be periodic, because of the anti-periodic b.c. (30). On the other hand, it is not hard to show that $\phi_{per} := \phi - \Phi x/L_x$ is x -periodic. In fact, this function solves the Laplace equation $\nabla^2 \phi_{per} = 0$ in Ω with the mixed boundary conditions

$$\frac{\partial \phi_{per}}{\partial n} = -\frac{\Phi}{L_x} n_x \Big|_{S_w}, \quad \phi_{per} = 0 \Big|_{S_{in}}, \quad \phi_{per} = 0 \Big|_{S_{out}}.$$

The solution of this problem is unique and x -periodic, vanishing on $S_{in} = S_{out}$. Furthermore, $\nabla \phi_{per} = \nabla \phi - \Phi/L_x$ so that the preceding discussion shows that ϕ_{per} is a C^∞ function on the entire flow domain Ω . We thus conclude that ϕ is the sum of a (smooth) periodic function and a function linear in x :

$$\phi = \phi_{per} + \Phi x/L_x$$

This fact will prove important in our derivation below.

With these results in hand we can essentially repeat the construction of Huggins⁵. We note here just the key differences. One can define $\mathbf{u}_\omega = \mathbf{u} - \mathbf{u}_\phi$ as before, but now \mathbf{u}_ω satisfies the non-flow-through constraints (20) only at S_w and not at $S_{in} = S_{out}$. However, the condition (32) that \mathbf{u}_ϕ carries the total mass flux still yields the weaker result that

$$\int_{S_{in}} \mathbf{u}_\omega \cdot \hat{\mathbf{n}} dA = \int_{S_{out}} \mathbf{u}_\omega \cdot \mathbf{n} dA = 0. \quad (38)$$

This suffices to imply that the potential and vortical fields are orthogonal, as the following brief calculation shows:

$$\begin{aligned} \int_{\Omega} \mathbf{u}_\phi \cdot \mathbf{u}_\omega dV &= - \int_{S_{in}} \phi \mathbf{u}_\omega \cdot \mathbf{n} dA - \int_{S_{out}} \phi \mathbf{u}_\omega \cdot \mathbf{n} dA \\ &\quad - \int_{S_w} \phi \mathbf{u}_\omega \cdot \mathbf{n} dA \\ &= \frac{1}{2} \Phi(t) \int_{S_{in}} \mathbf{u}_\omega \cdot \mathbf{n} dA - \frac{1}{2} \Phi(t) \int_{S_{out}} \mathbf{u}_\omega \cdot \mathbf{n} dA = 0. \end{aligned} \quad (39)$$

Note that neither smoothness of ϕ nor even flatness of the sections S_{in} , S_{out} were required here. The other key step in the derivation of Huggins⁵ where the constraints (20) were used was in the calculation (23) of the balance equation for E_ω , where they were invoked to eliminate the boundary terms at S_{in} and S_{out} involving h_ω . In fact, the weaker conditions (38) again suffice, if one recalls that

$$h_\omega = h + \partial_t \phi = p + \frac{1}{2} |\mathbf{u}|^2 + Q + \partial_t \phi \quad (40)$$

so that h_ω is the sum of a smooth, x -periodic part $h_{\omega,per} = p + \frac{1}{2} |\mathbf{u}|^2 + Q_{per} + \partial_t \phi_{per}$ and a linear part $h_{\omega,lin} = \Phi x/L_x - \gamma x$. In that case, the periodic part gives no contribution and the linear part contributes zero also because

$$\rho \int_{S_{in}} h_{\omega,lin} \mathbf{u}_\omega \cdot \mathbf{n} dA + \rho \int_{S_{out}} h_{\omega,lin} \mathbf{u}_\omega \cdot \mathbf{n} dA$$

$$\begin{aligned}
&= -\frac{1}{2}(\dot{\Phi} - \gamma L_x)\rho \int_{S_{in}} \mathbf{u}_\omega \cdot \mathbf{n} dA \\
&\quad + \frac{1}{2}(\dot{\Phi} - \gamma L_x)\rho \int_{S_{out}} \mathbf{u}_\omega \cdot \mathbf{n} dA = 0. \quad (41)
\end{aligned}$$

Here we required flatness of S_{in} , S_{out} so that $h_{\omega,lin}$ is constant on those surfaces and continuity of $\mathbf{u}_\omega = \mathbf{u} - \mathbf{u}_\phi$ at $S_{in} = S_{out}$ to cancel the contribution from $h_{\omega,per}$. In conclusion, the balance equation (23) for E_ω again holds, and all of the rest of the derivation is identical to that of Huggins⁵.

There are a few further simplifications compared with the construction of Huggins⁵ due to the fact that both h and h_ω are now smooth, x -periodic functions plus a part which is linear in x . Thus, rate of work \mathcal{W} by total pressure head defined in (13) now becomes

$$\mathcal{W} = \gamma(t)L_x J = (\Delta h)J$$

where we have defined $\Delta h = \gamma L_x$ as the drop in total pressure. Likewise, the work done by the total rotational pressure is

$$\mathcal{W}_\omega = [(\Delta h) - \dot{\Phi}]J = (\Delta h_\omega)J,$$

so that the detailed *JA*-relation now becomes simply

$$\mathcal{T} = (\Delta h_\omega)J = (\Delta h)J - \mathcal{W}_\phi, \quad (42)$$

The rate of work by the potential flow simplifies also as

$$\mathcal{W}_\phi = J\dot{\Phi} = JJ/J_* = \dot{E}_\phi, \quad (43)$$

For the special case of a flow with a mass flux constant in time, $dJ/dt = 0$, one gets furthermore $\Delta h_\omega = \Delta h$ and $\mathcal{T} = (\Delta h)J$.

It is also instructive to consider the canonical case of channel flow with flat plane-parallel walls and $\mathbf{f} = \mathbf{0}$. In that case, as previously noted, our construction yields $\phi(t) = U(t)x$ and $\mathbf{u}_\phi = U(t)\hat{\mathbf{x}}$ is spatially constant. It follows then from the alternative formula (28) for \mathcal{T} in the Introduction that

$$\mathcal{T} = \rho U \int_{S_w} \tau_{xy}^w dA, \quad (44)$$

which is the energy dissipated by viscous wall drag. Thus, in this particular case, both the work done against rotational pressure and the dissipation by drag are instantaneously related to vorticity flux across the channel. The transfer term likewise simplifies to

$$\mathcal{T} = -\rho U \int_{\Omega} \Sigma_{yz} dV = -\rho U \int_{\Omega} (\omega_z v - \omega_y w - v \partial_y \omega_z) dV$$

where note that $\int_{\Omega} \partial_z \omega_y dV = 0$ because of the spanwise periodic b.c. Note further because of the vector calculus identity

$$\omega_z v - \omega_y w = -\partial_x(u^2) - \partial_y(vu) - \partial_z(wu) + \frac{1}{2}\partial_x(u^2 + v^2 + w^2) \quad (45)$$

and the assumed boundary conditions that the net contribution to \mathcal{T} from the nonlinear term *vanishes*, when integrated over the flow volume. This vanishing value is special to channel flow with flat, parallel walls, because of the high degree of symmetry of this flow, whereas the nonlinear contribution to

the *JA*-relation is generally not zero (e.g. see next section). Integrating the remaining term $v \partial_y \omega_z$ in y directly recovers (44) and the detailed *JA*-relation reduces to an instantaneous version of the time-average result for turbulent channel flow, $\langle \Sigma_{yz} \rangle = -u_\tau^2/h$, previously discussed in the literature^{8,14,15}. Note however that the time-average $\langle \omega_z v - \omega_y w \rangle(y) \neq 0$ and this term is crucial to give a y -independent constant mean total flux, although contributions from negative and positive signs of the mean nonlinear flux exactly cancel when integrated over y -locations. See Kumar, Meneveau, and Eyink¹⁵ for more discussion of the physical mechanisms.

IV. NUMERICAL RESULTS FOR A FLAT-WALL CHANNEL WITH A SMOOTH BUMP

In this section we present a numerical application of our new detailed *JA* relation. In order to investigate flow separation and its contribution to drag, we have selected for study a streamwise-periodic channel flow with plane-parallel walls modified by addition of a smooth bump or ridge at the wall, with a cosine profile in the streamwise direction over a complete period, from minimum to minimum, and spanwise constant. See Fig. 5 for a sideview of the geometry. We keep the bulk flow velocity U constant, for ease of demonstration, with the pressure gradient $\gamma(t)$ which drives the flow varying to maintain the constant flow rate. We take the x -direction as streamwise, y -direction as wall-normal and z -direction as spanwise. We consider a domain of size $(L_x, L_y, L_z) = (1, 1, 0.5)$ in arbitrary units and the height and width of the cosine bump are $0.1L_x$ and $0.5L_x$, respectively. We initialize the velocity field with a constant value $\mathbf{u} = (U, 0, 0)$, The Reynolds number based on bulk velocity U and channel height L_y is thus constant at $Re = UL_y/\nu = 975$, which results in an unsteady laminar flow, sufficient to drive flow separation from the bump and to generate a rotational wake.

Case	Nx	Ny	Nz	RelErr(%)
1	50	50	25	11.7
2	80	80	40	7.88
3	160	160	81	4.38
4	216	216	108	3.56

TABLE I: The effect of grid size on maximum error

To compute this flow numerically we use the laminar *pimpleFoam*⁴⁶ solver from *OpenFOAM*⁴⁷, with a body-fitted structured mesh of hexahedral cells and a range of mesh sizes listed in Table I. A convergence study shows that the results are accurate within a few percent for the finest mesh $(N_x, N_y, N_z) = (216, 216, 108)$ (see below) and all concrete results presented here are for that resolution. Numerical field values are output at time intervals of $\Delta t U/L_x = 0.195$ starting at $tU/L_x = 0.195$. Our goal is to numerically evaluate the detailed *JA*-relation (42), which here takes the concrete form

$$\gamma(t)L_x J = - \int_{\Omega} \rho \mathbf{u}_\phi \cdot (\mathbf{u} \times \boldsymbol{\omega} - \mathbf{v} \nabla \times \boldsymbol{\omega}) dV := \mathcal{T}(t) \quad (46)$$

since $dJ/dt = 0$ and $\mathbf{f} = \mathbf{0}$. The volume-integral in (46) was computed numerically by a Riemann sum where each cell is associated with a single value and all values are multiplied by cell volume and added to get integrals. To obtain $\mathbf{u}_\phi = \Phi(t)\mathbf{u}_\phi^*$, the geometry-dependent dimensionless potential ϕ_* satisfying b.c. (33) was calculated by solving the Laplace equation using the same mesh. The results are shown in Fig. 5, which plots ϕ_* as a color map and representative streamlines. The prefactor $\Phi(t)$ is time-independent for this flow with constant bulk velocity and fixed by the relation $\Phi = J/J_*$. All space-gradients such as $\boldsymbol{\omega} = \nabla \times \mathbf{u}$ and $\nabla \times \boldsymbol{\omega}$ were calculated by central differences. We find that the maximum relative error between the LHS and RHS of the JA relation (46), or $RelErr(\%) = 100 \max_t \left| 1 - \frac{\mathcal{T}(t)}{J_* \gamma(t)} \right|$ decreases with mesh resolution, as shown in the final column of Table I. We deemed the maximum error $\leq 3.56\%$ achieved at our highest resolution to be adequate for the purposes of this study.

More detailed information about accuracy is afforded by the plots in Fig 6 of the time series of the driving pressure-gradient $\gamma(t)$ and of the transfer term $\mathcal{T}(t)$ in the detailed JA-relation, suitably non-dimensionalized, which agree quite well over the entire recorded time period. However, in addition to numerical validation, further information about the physics is provided by the plots in Fig 6 of the separate contributions to $\mathcal{T}(t)$ arising from viscous and nonlinear vorticity transport. At the moderate Reynolds number of the simulation, the viscous contribution is largest and the nonlinear contribution only about half as large. On the other hand, the instantaneous drag as measured by $\gamma(t)$ exhibits distinctive oscillations, which are contributed entirely by the nonlinear transport term in $\mathcal{T}(t)$ whereas the viscous term decays monotonically in time. We argue that the local maxima in drag are due to periodic episodes of strong vortex shedding from the smooth bump, whereas the local minima are due to episodes of weaker shedding. We present several pieces of evidence to support this interpretation.

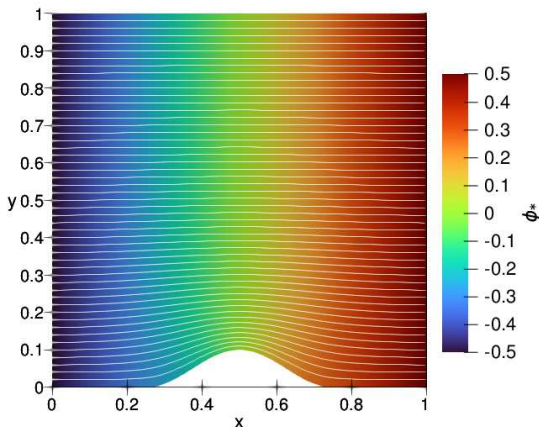


FIG. 5: Dimensionless background potential ϕ_* and its streamlines.

One such piece of evidence comes from an additional exact relation derived from the constraint $\frac{1}{L_x L_y L_z} \int_{\Omega} \mathbf{u} dV = U \hat{\mathbf{x}}$

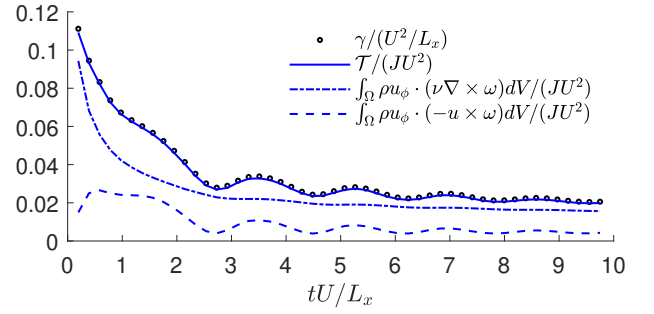


FIG. 6: Time series of terms in the detailed JA relation (Eq. 46) for flow past a bump in a periodic channel with a constant flow rate ($dJ/dt = 0$), also showing separate viscous and nonlinear contributions to the transfer term.

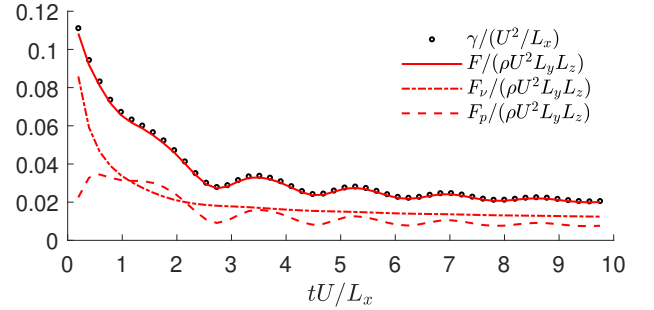


FIG. 7: Time series of terms in the global momentum balance, the net drag force $F_x(t)$ on the wall and the instantaneous pressure gradient $\gamma(t)$, also showing separate contributions from skin friction and pressure to drag force.

and the global momentum balance obtained by integrating the governing Navier-Stokes equation over the flow domain:

$$\int_{S_w} (-P\mathbf{n} + \rho\boldsymbol{\tau}_w) dA + \dot{J}(t)L_x = \rho\gamma(t)L_x L_y L_z \hat{\mathbf{x}}. \quad (47)$$

In the case considered here $dJ/dt = 0$, so that global momentum balance reduces to the relation

$$\mathbf{F}(t) := \int_{S_w} (-P\mathbf{n} + \rho\boldsymbol{\tau}_w) dA = \rho\gamma(t)L_x L_y L_z \hat{\mathbf{x}}, \quad (48)$$

where the lefthand side is the instantaneous drag force exerted by the fluid on the channel walls and the righthand side is the instantaneous force applied by the external pressure gradient to the fluid. Plotted in Fig. 7 are the times series of the x -components of the two sides of Eq.(48), suitably normalized, whose excellent agreement again validates our numerical solution. More physically informative are the plots in Fig. 7 of the separate contributions to the drag force from the viscous skin friction and the pressure (form drag), which show remarkably similar (but not identical) behaviors as the viscous and nonlinear transport contributions to the JA-relation as plotted in Fig. 6. The similarity of the viscous contributions is unsurprising, as we have already noted in Eq.(28) that

$$\int_{\Omega} \mathbf{u}_\phi \cdot \nu \nabla \times \boldsymbol{\omega} dV = \int_{\partial\Omega} \mathbf{u}_\phi \cdot \boldsymbol{\tau}_w dA. \quad (49)$$

by a simple application of the divergence theorem. Thus, the viscous term in the JA transfer term coincides with the viscous term in the drag force after substituting \mathbf{u}_ϕ for $U\hat{\mathbf{x}}$. Since Fig. 5 shows that \mathbf{u}_ϕ and $U\hat{\mathbf{x}}$ are quite similar, it is understandable that the two viscous contributions are closely correlated.

We cannot find any such direct correspondence between the nonlinear term $\mathcal{T}_{nl}(t)$ and the form drag $F_{px}(t)$, but it is well-known that large form drag is associated to earlier or stronger shedding of vorticity by flow separation. Thus, the similar oscillations observed in both the form drag and the nonlinear transfer term are likely both due to oscillations in separation. Boundary-layer separation can in fact be verified in this flow by visualization of spatial fields in Fig. 8. For simplicity we have chosen to visualize a late time $tU/L_x = 9.75$ when the flow has become nearly steady and we plot fields in the vertical xy -plane at the spanwise midsection $z = 0.25$. The plot of the streamwise velocity u in Fig. 8a is relatively uninformative, showing just a slightly elevated region of reduced streamwise velocity downstream of the bump. However, the plot of the wall-normal velocity v in Fig. 8b shows a clear upward jet just upstream of the bump, while just downstream there is a bipolar pattern of downflow followed by upflow indicative of a recirculation bubble. Most compelling is the plot of the spanwise vorticity in Fig. 8c which shows a strong sheet of negative spanwise vorticity on the upstream face of the bump associated to a viscous boundary layer which is then shed into the flow downstream of the bump. On the downstream face of the bump the vorticity is instead positive, indicating a recirculation bubble. In fact, we see such clear evidence of flow separation at all recorded times.

To get physical understanding of the relation of drag to such vorticity dynamics, we can visualize the integrand appearing in the spatial integral which defines the transfer term $\mathcal{T}(t)$ in the detailed JA-relation of Eq.(46). We plot this integrand in Fig. 9 at the same time $tU/L_x = 9.75$ and in the xy -plane at the same spanwise position $z = 0.25$ as the flow fields plotted in Fig. 8, so that the two may be compared directly. We note, however, that while our flow varies substantially in time, it is rather spanwise homogeneous, so that the plots in xy -planes at other spanwise positions are very similar. We plot in Fig. 9a the viscous contribution to the integrand, in Fig. 9b the nonlinear contribution, and in Fig. 9c the combined integrand, representing local total flux of vorticity across flowlines of the Euler potential. We discuss each of the plots in turn.

The viscous contribution to the JA-transfer term plotted in Fig 9a can be readily understood, because Huggins' flux tensor Σ appearing in (15) for flux normal to the wall is exactly equal to the Lighthill boundary vorticity source σ , or

$$\Sigma^\top \mathbf{n} = \sigma = \mathbf{v}\mathbf{n} \times (\nabla \times \boldsymbol{\omega}), \quad (50)$$

where the relevant expression for σ is that of Lyman⁴⁸ rather than the alternative expression of Lighthill¹⁰ and Panton⁴⁹. Thus, the viscous vorticity flux in the flow interior directly continues that from the solid wall. Crucially, all transfer terms plotted in Fig. 9 arise from *wall-normal flux of spanwise vorticity*, since the potential flow-lines are parallel to the wall and furthermore $\boldsymbol{\omega} \cdot \mathbf{n} = 0$ and $\mathbf{n} \cdot \boldsymbol{\sigma} = 0$, i.e. wall-normal vorticity and its fluxes are negligible in the vicinity of the surface.

However, as also emphasized by Lighthill¹⁰ and especially by Morton⁵⁰, vorticity generation at the surface is an essentially inviscid process driven by tangential pressure gradients, as shown by the equivalent formula

$$\boldsymbol{\sigma} = -\mathbf{n} \times \nabla p. \quad (51)$$

Thus, the favorable pressure-gradient on the upstream side of the bump generates negative spanwise vorticity, whereas the adverse pressure-gradient on the downstream side generates positive spanwise vorticity. For plots of the pressure fields, see Supplementary Materials, §IV. These signs are observed both in the plot of spanwise vorticity in Fig 8c and in the plot of the viscous transfer in Fig. 9a. As emphasized by Lighthill¹⁰, however, the change of sign of σ_z occurs earlier than the change of sign of ω_z (the point of separation), because it takes some time for the reversed positive flux to subtract the negative vorticity already present, and this delay is clearly observed in Figs. 8c & 9a. The viscous transport of spanwise vorticity into the flow interior continues that at the surface but decreases rapidly as vorticity gradients drop off.

The nonlinear contribution to the JA-transfer term plotted in Fig 9b is the dominant one through the bulk of the flow, but consists of two large lobes of opposite sign upstream and downstream of the bump, which substantially cancel. Thus, at the moderate Reynolds number of this simulation, nonlinear transfer provides only 21.4% to the instantaneous drag at $tU/L_x = 9.75$ and viscous transfer the remaining 78.6%. The dominant contribution to the nonlinear vorticity flux in the region above the bump is the streamwise advection of spanwise vorticity, $\Sigma_{xz} \simeq u\omega_z$, as may be seen from the plots in Fig. 8. The streamwise velocity plotted in Fig. 8a is more than an order of magnitude larger than the wall-normal component in Fig. 8b, while the spanwise velocity (not shown) is even smaller. The largest component of vorticity is by far the spanwise one ω_z and, in the region just above the bump, its sign is negative. This is the dominant sign of vorticity shed from the bump which then, given the periodic boundary conditions, recirculates through the domain in the streamwise direction. Note, incidentally, that the dominant shedding of negative spanwise vorticity is directly related to form drag on the bump by the Lighthill-Morton relation (51), since the smaller flux of positive vorticity after separation implies that the pressure never fully recovers its upstream value. The flux Σ_{xz} contributes to transfer across the potential streamlines because the latter bend vertically upward just upstream of the bump and vertically downward just downstream; see Fig. 5. These considerations easily account for the observed signs of the two lobes in Fig 9b⁵¹. The reason that the positive/drag-producing lobe downstream dominates over the negative/drag-reducing lobe upstream is that the streamwise vorticity is strongest immediately after it is shed, whereas the vorticity periodically re-entering the flow domain upstream is diffused and weaker.

Combining the viscous and nonlinear contributions yields the total transfer integrand plotted in Fig 9c. A very simple and intuitive picture thereby emerges for the origin of drag via vorticity dynamics. Negative spanwise vorticity is generated by the favorable pressure gradient on the upstream side of the bump, while a smaller amount of positive vorticity is gener-

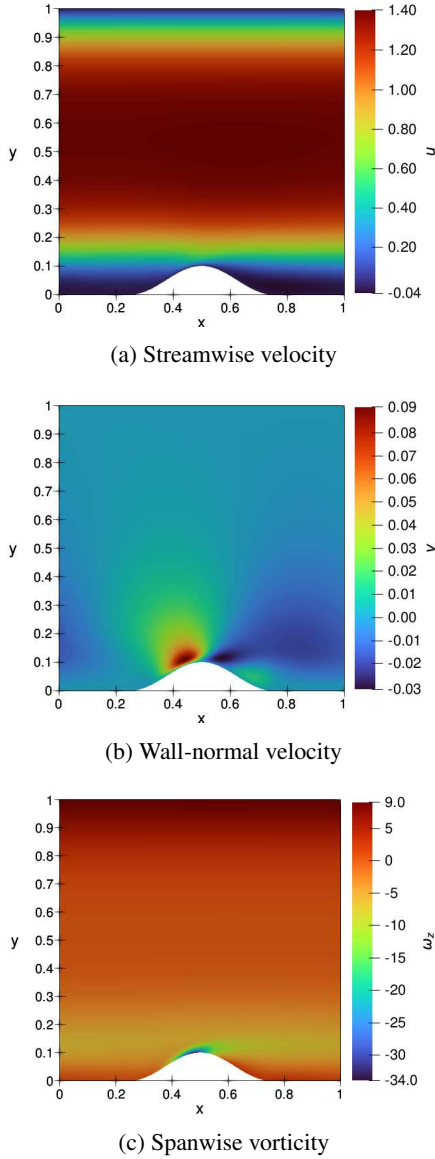


FIG. 8: Instantaneous velocity fields, (a) streamwise and (b) wall-normal, normalized by U , and (c) spanwise vorticity field normalized by U/L_x , at $tU/L_x = 9.75$, $z = 0.25$.

ated by the adverse pressure gradient downstream. This vorticity viscously diffuses into the flow interior where nonlinear advection then takes over, convecting the excess negative spanwise vorticity downstream. Drag is produced as the negative spanwise vorticity crosses the streamlines of the background Euler potential. This picture directly relates the nonlinear flux contribution in the JA-relation to form drag, since the latter results from the shedding of excess negative spanwise vorticity, and we can therefore understand the high correlation between the two terms observed in Figs. 6 & 7. Note that the results that we have observed here for $tU/L_x = 9.75$ are quite general and hold at all recorded times. Only the strength of vortex shedding varies with time, with strong shedding at times of local maximum drag in Figs. 6 & 7 and weak

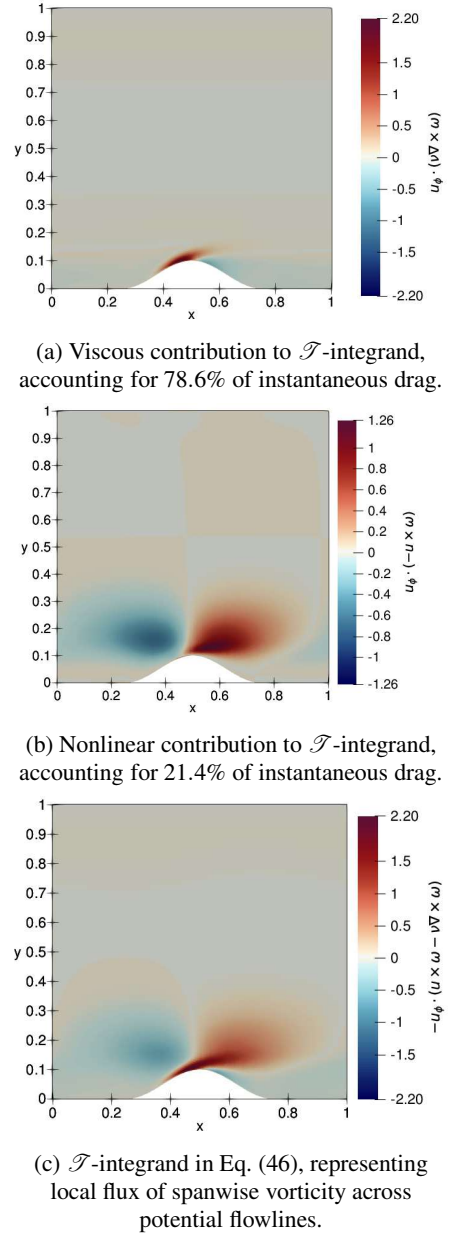


FIG. 9: Instantaneous fields of (c) the integrand of \mathcal{F} in the detailed JA-relation (46), and (a) viscous and (b) nonlinear contributions to the integrand, all normalized by $\rho U^3/L_x$. Fields are shown for $tU/L_x = 9.75$, $z = 0.25$.

shedding at times of local minimum drag. See Supplemental Material, §II-III, in particular for a comparison of the two times $tU/L_x = 3.51$ and $tU/L_x = 4.485$ corresponding to a local maximum and minimum, respectively.

Although we have considered only a single flow geometry at a single Reynolds number, many of our conclusions are much more general. In fact, the JA-relation has recently been evaluated by Du and Zaki⁵² for external flow past spherical and spheroidal bodies and their results are very similar to ours. Spanwise (azimuthal) vorticity is generated in that flow principally by favorable pressure gradients on the body surface.

This azimuthal vorticity diffuses outward from the sphere by viscosity but is shed rapidly into the flow by boundary-layer separation. Nonlinear advection takes over, with convection, stretching, and twisting of vorticity, and resultant drag is produced by the integrated flux of the azimuthal vorticity across the streamlines of the background Euler potential. One difference is that Du and Zaki⁵² do not see an “anti-drag” lobe upstream of the body similar to ours in Fig. 9c, because they do not use periodic boundary conditions and their inflow has negligible vorticity. In addition, their simulations are at higher Reynolds numbers than ours and the wake behind their body is fully turbulent. The vorticity dynamics in wall-bounded turbulent flows is more complex than what we observe in our laminar flow. As just one example, we observe nonlinear vorticity transfer in our flow to be dominated by streamwise advection of spanwise vorticity across potential streamlines, but the spanwise transport of wall-normal vorticity is found to play an essential role in turbulent channel-flow in the buffer layer and throughout the log-layer, related to velocity-correlated vortex-stretching¹⁵. Nevertheless, the drag in turbulent wall-bounded flows is due also to the cross-stream flux of spanwise vorticity^{8,14,15}. Thus, the Josephson-Anderson relation reveals a deep underlying unity in the origin of drag via vorticity dynamics, encompassing flows both internal and external, both laminar and turbulent, both classical and quantum.

V. CONCLUSIONS

We have reviewed in this paper the detailed Josephson-Anderson relation for instantaneous drag first derived by Huggins⁵ for internal flows through general channels and we have explained how this result provides the exact analogue of the drag formulas for external flow past bodies derived by Wu³⁶, Lighthill^{35,37}, Howe¹³, Eyink¹¹, and others¹². In all of these works, instantaneous drag is divided into a potential part and an “effective” rotational part that arises from vorticity flux across streamlines of the background potential Euler flow. However, we showed that the original relation of Huggins⁵ suffers from significant problems when applied to classical turbulence and, in particular, his prescription for the background potential introduces a spurious vortex sheet for the streamwise periodic flows that are widely employed in numerical simulations. We proposed instead a reference potential Euler flow whose mass flux matches that of the total velocity field, while also ensuring that the vortical and potential velocity fields are orthogonal. The main theoretical result of our paper is the new detailed Josephson-Anderson relation (42) for streamwise periodic flows, which equates the instantaneous rate of work \mathcal{W}_ω due to rotational pressure, given by (14), and the integrated flux of vorticity \mathcal{T} across potential streamlines, given by (15). We finally illustrated the utility of this relation by the example of Poiseuille flow in a flat-wall channel with a single smooth bump at the wall. The main physical conclusion of our work is contained in the numerical results plotted in Fig. 9 and the resulting explanation of the origin of drag in terms of vorticity shed due to flow separation from the bump.

It is interesting to ask how our results are related to the

views of Feynman on the role of vortex reconnections in superfluid turbulence. Posing the question “What can eventually become of the kinetic energy of the vortex lines?,” Feynman¹⁹ argued that “the lines (which are under tension) may snap together and join connections a new way” and he proposed a picture of a sequence of reconnections as a path to dissipation of vortex energy into elementary excitations. A modern version of this picture is the Kelvin wave cascade generated by vortex reconnections^{53,54}. In fact, the experiments of Bewley *et al.*¹⁶ and Fonda, Sreenivasan, and Lathrop^{17,18} have visualized the quantized vortex lines in superfluid turbulence and observed their reconnection dynamics. We agree with the view that vortex reconnection is an essential part of turbulence, not only in quantum fluids but also in classical fluids. A major difference is that classical vorticity distributions are continuous and Newtonian viscosity allows vorticity to diffuse like smoke through the fluid. However, the stochastic Lagrangian description of classical vortex motion via a Feynman-Kac representation shows that line-reconnection occurs everywhere in classical turbulent flows, continuously in time⁵⁵⁻⁵⁷. On the other hand, focusing on the small-scale dissipation of fluid-mechanical vortex motions into heat, in our opinion, misses an essential element of turbulent dissipation. Referring to classical fluid turbulence driven by a pressure gradient, Feynman¹⁹ argued that “The vortex lines twist about in an ever more complex fashion, increasing their length at the expense of the kinetic energy of the main stream.” In fact, complex, irregular motion is not sufficient to explain turbulent dissipation in such flows. The essential new idea supplied by Josephson³ and Anderson⁴, which was missed by Feynman, is that organized *cross-stream vortex motion* and not just random stretching and reconnection is required to explain the enhanced energy dissipation in wall-bounded turbulence of both quantum and classical fluids.

In our opinion, this point is likely of key importance in the explanation of the *anomalous energy dissipation* for incompressible fluid turbulence, which was proposed by Onsager^{39,40,41} and which was the subject of pioneering empirical investigations by Sreenivasan^{25,26} and Meneveau and Sreenivasan²⁷. Various experiments^{58,59} have shown that the presence of wall-roughness is crucial for the existence of a dissipative anomaly and some phenomenological scaling theories^{60,61} lead to the same conclusion. Experimental visualizations of flow around individual cubic roughness elements in a turbulent duct flow⁶² exhibit similar features as our smooth bump, with form drag, flow separation and vortex shedding into the interior. It thus seems likely that such phenomena must persist in order to produce a dissipative anomaly in the infinite Reynolds number limit. It is known from experimental studies of Sreenivasan²⁰ and Sreenivasan and Sahay²¹ that viscous effects persist in the log-layer of smooth-wall turbulent flows up to the location of peak Reynolds stress and mean vorticity flux in particular is dominated by viscous transport over this range^{8,15}. Mathematical analysis^{38,63,41} shows that anomalous viscous transport of vorticity outward from the wall may in fact persist in the infinite-Reynolds limit, and persistent shedding of vorticity and resultant form drag seem the most plausible mechanism for anomalous energy dissipation

in rough-walled turbulent flows.

In future work, we hope to apply our new detailed Josephson-Anderson relation to several problems of current interest. Our work gives a new perspective on the problem of turbulent drag reduction which we plan to pursue, in particular for polymer additives⁶⁴. Note that the polymer stress contributes simply a body force $\mathbf{f} = \nabla \cdot \boldsymbol{\tau}_p$ in the Navier-Stokes equation (1) and the detailed JA-relation hence applies directly to viscoelastic fluids. Another problem of practical importance is the parameterization of surface drag in rough-walled turbulent flows, which has already been investigated⁶⁵ by the Force Partition Method (FPM)^{66,67} which is closely related to the Josephson-Anderson relation. The relationship of these two approaches deserves to be discussed at length, but we just note here that FPM derives an exact expression for form drag as a spatial integral of the second-order invariant $Q = -(1/2)\text{Tr}[(\nabla\mathbf{u})^2]$ and the viscous acceleration $\nu\Delta\mathbf{u}$ weighted by a scalar potential ϕ and its gradient $\nabla\phi$, respectively. While such an integral relation is similar in form to the JA relation, FPM uses a different potential, yields results for the pressure contribution to drag only, and has the aim to relate form drag to Q -structures rather than to vorticity dynamics. Another approach to derive exact formulas for skin friction is that of Fukagata, Iwamoto, and Kasagi⁶⁸, yielding the so-called FIK identity, and a vorticity-based version in particular relates the skin friction to velocity-vorticity correlations⁶⁹, similar to the JA-relation. However, FIK-type identities apply only to flat-walled flows without form drag and yield a result only for homogeneous averages. The detailed Josephson-Anderson relation derived by Huggins⁵ and extended in this work, by contrast, describes the total drag from both skin friction and form drag and applies instantaneously in time.

ACKNOWLEDGMENTS

We thank Y. Du, N. Goldenfeld, J. Katz, C. Meneveau, R. Mittal and T. Zaki for discussions of this problem and of their related results. We wish to express our gratitude to K. R. Sreenivasan for his friendship over many years and for his leadership in science, which we hope will continue well into the future. Finally, we thank the Simons Foundation for support of this work through the Targeted Grant No. MPS-663054, “Revisiting the Turbulence Problem Using Statistical Mechanics” and also the Collaboration Grant No. MPS-1151713, “Wave Turbulence”.

- ¹R. E. Packard, “The role of the Josephson-Anderson equation in superfluid helium,” *Reviews of Modern Physics* **70**, 641 (1998).
- ²E. Varoquaux, “Anderson’s considerations on the flow of superfluid helium: Some offshoots,” *Reviews of Modern Physics* **87**, 803 (2015).
- ³B. D. Josephson, “Potential differences in the mixed state of type II superconductors,” *Phys. Lett.:(Netherlands)* **16** (1965).
- ⁴P. W. Anderson, “Considerations on the flow of superfluid helium,” *Rev. Mod. Phys.* **38**, 298–310 (1966).
- ⁵E. R. Huggins, “Energy-dissipation theorem and detailed Josephson equation for ideal incompressible fluids,” *Phys. Rev. A* **1**, 332–337 (1970).
- ⁶W.-K. Kwok, U. Welp, A. Glatz, A. E. Koshelev, K. J. Kihlstrom, and G. W. Crabtree, “Vortices in high-performance high-temperature superconductors,” *Rep. Prog. Phys.* **79**, 116501 (2016).

- ⁷A. Glatz, I. A. Sadovskyy, U. Welp, W.-K. Kwok, and G. W. Crabtree, “The quest for high critical current in applied high-temperature superconductors,” *J. Supercond. Novel Mag.* **33**, 127–141 (2020).
- ⁸G. L. Eyink, “Turbulent flow in pipes and channels as cross-stream “inverse cascades” of vorticity,” *Physics of Fluids* **20**, 125101 (2008).
- ⁹G. I. Taylor, “The transport of vorticity and heat through fluids in turbulent motion,” *Proceedings of the Royal Society of London. Series A, Containing Papers of a Mathematical Character*, edited by L. Rosenhead (Oxford University Press, Oxford, 1963) pp. 46–113.
- ¹⁰M. J. Lighthill, “Introduction: Boundary layer theory,” in *Laminar Boundary Theory*, edited by L. Rosenhead (Oxford University Press, Oxford, 1963) pp. 46–113.
- ¹¹G. L. Eyink, “Josephson-Anderson relation and the classical D’Alembert paradox,” *Phys. Rev. X* **11**, 031054 (2021).
- ¹²A. Biesheuvel and R. Hagmeijer, “On the force on a body moving in a fluid,” *Fluid Dynamics Research* **38**, 716 (2006).
- ¹³M. S. Howe, “On the force and moment on a body in an incompressible fluid, with application to rigid bodies and bubbles at high and low Reynolds numbers,” *Q. J. Mech. Appl. Math.* **48**, 401–426 (1995).
- ¹⁴E. R. Huggins, “Vortex currents in turbulent superfluid and classical fluid channel flow, the Magnus effect, and Goldstone boson fields,” *Journal of Low Temperature Physics* **96**, 317–346 (1994).
- ¹⁵S. Kumar, C. Meneveau, and G. L. Eyink, “Vorticity cascade and turbulent drag in wall-bounded flows: plane Poiseuille flow,” *Journal of Fluid Mechanics* **974**, A27 (2023).
- ¹⁶G. P. Bewley, M. S. Paoletti, K. R. Sreenivasan, and D. P. Lathrop, “Characterization of reconnecting vortices in superfluid helium,” *Proceedings of the National Academy of Sciences* **105**, 13707–13710 (2008).
- ¹⁷E. Fonda, K. R. Sreenivasan, and D. P. Lathrop, “Sub-micron solid air tracers for quantum vortices and liquid helium flows,” *Review of Scientific Instruments* **87** (2016).
- ¹⁸E. Fonda, K. R. Sreenivasan, and D. P. Lathrop, “Reconnection scaling in quantum fluids,” *Proceedings of the National Academy of Sciences* **116**, 1924–1928 (2019).
- ¹⁹R. P. Feynman, “Application of quantum mechanics to liquid helium,” in *Progress in Low Temperature Physics*, Vol. 1, edited by C. Gorter (North-Holland, Amsterdam, 1955) pp. 17–51.
- ²⁰K. R. Sreenivasan, “A unified view of the origin and morphology of the turbulent boundary layer structure,” in *Turbulence Management and Relaminarisation: Proceedings of the IUTAM Symposium*, B. IUTAM Symposia, edited by H. Liepmann and R. Narashima (Springer, Berlin Heidelberg, 1987) pp. 37–61.
- ²¹K. R. Sreenivasan and A. Sahay, “The persistence of viscous effects in the overlap region, and the mean velocity in turbulent pipe and channel flows,” in *Self-sustaining Mechanisms of Wall Turbulence*, *Advances in fluid mechanics*, Vol. 15, edited by R. Panton (Computational Mechanics Pub., 1997) pp. 253–272.
- ²²X. Chen and K. R. Sreenivasan, “Reynolds number scaling of the peak turbulence intensity in wall flows,” *Journal of Fluid Mechanics* **908**, R3 (2021).
- ²³X. Chen and K. R. Sreenivasan, “Law of bounded dissipation and its consequences in turbulent wall flows,” *Journal of Fluid Mechanics* **933**, A20 (2022).
- ²⁴K. R. Sreenivasan and C. M. White, “The onset of drag reduction by dilute polymer additives, and the maximum drag reduction asymptote,” *Journal of Fluid Mechanics* **409**, 149–164 (2000).
- ²⁵K. R. Sreenivasan, “On the scaling of the turbulence energy dissipation rate,” *The Physics of fluids* **27**, 1048–1051 (1984).
- ²⁶K. R. Sreenivasan, “An update on the energy dissipation rate in isotropic turbulence,” *Physics of Fluids* **10**, 528–529 (1998).
- ²⁷C. Meneveau and K. Sreenivasan, “The multifractal nature of turbulent energy dissipation,” *Journal of Fluid Mechanics* **224**, 429–484 (1991).
- ²⁸E. R. Huggins, “Dynamical theory and probability interpretation of the vorticity field,” *Physical Review Letters* **26**, 1291 (1971).
- ²⁹L. Kelvin, “On vis-viva of a liquid in motion, Cambridge and Dublin Math. J. (1849),” in *Mathematical and Physical Papers: Collected from Different Scientific Periodicals from May, 1841, to the Present Time*, Vol. I (C. J. Clay & Sons, Cambridge University Press, 1882).
- ³⁰H. Lamb, *Hydrodynamics* (University Press, 1924).
- ³¹G. K. Batchelor, *An Introduction to Fluid Dynamics* (Cambridge University Press, 2000).

- ³²J.-Z. Wu, H.-Y. Ma, and M.-D. Zhou, *Vorticity and vortex dynamics* (Springer Science & Business Media, 2007).
- ³³J. I. R. d'Alembert, "Theoria resistientiae quam patitur corpus in fluido motum, ex principiis omnino novis et simplissimis deducta, habita ratione tum velocitatis, figurae, et massae corporis moti, tum densitatis compressionis partium fluidi," manuscript at Berlin-Brandenburgische Akademie der Wissenschaften, Akademie-Archiv call number: I-M478 (1749).
- ³⁴J. I. R. d'Alembert, "Paradoxe proposé aux géomètres sur la résistance des fluides," in: *Opuscules mathématiques*, vol. 5 (Paris), Memoir XXXIV, Section I, 132–138 (1768).
- ³⁵M. J. Lighthill, *An Informal Introduction to Theoretical Fluid Mechanics*, IMA monograph series, Vol. 2 (Clarendon Press, 1986).
- ³⁶J. C. Wu, "Theory for aerodynamic force and moment in viscous flows," *AIAA Journal* **19**, 432–441 (1981).
- ³⁷J. Lighthill, "Fundamentals concerning wave loading on offshore structures," *Journal of Fluid Mechanics* **173**, 667–681 (1986).
- ³⁸H. Quan and G. L. Eyink, "Onsager theory of turbulence, the Josephson-Anderson relation, and the D'Alembert paradox," arXiv preprint arXiv:2206.05326 (2022).
- ³⁹L. Onsager, "Statistical hydrodynamics," *Nuovo Cimento, Suppl.* **6**, 279–287 (1949).
- ⁴⁰G. L. Eyink and K. R. Sreenivasan, "Onsager and the theory of hydrodynamic turbulence," *Reviews of modern physics* **78**, 87 (2006).
- ⁴¹G. Eyink, "Onsager's 'ideal turbulence' theory," *Journal of Fluid Mechanics* **988**, P1 (2024).
- ⁴²Y. Li, E. Perlman, M. Wan, Y. Yang, C. Meneveau, R. Burns, S. Chen, A. Szalay, and G. L. Eyink, "A public turbulence database cluster and applications to study lagrangian evolution of velocity increments in turbulence," *Journal of Turbulence* **9**, N31 (2008).
- ⁴³J. Graham, K. Kanov, X. I. A. Yang, M. Lee, N. Malaya, C. C. Lalescu, R. Burns, G. Eyink, A. Szalay, R. D. Moser, and C. Meneveau, "A web services accessible database of turbulent channel flow and its use for testing a new integral wall model for les," *Journal of Turbulence* **17**, 181–215 (2016).
- ⁴⁴The reflection symmetry of the domain is unnecessary to derive our new JA-relation, if the flow is forced by prescribing constant values of h_{in} on S_{in} and h_{out} on S_{out} , and these surfaces in that case may even be curved. This driving corresponds to solving the Poisson equation for pressure p with mixed Dirichlet-Neumann conditions of the form $p = h_{in} - (\frac{1}{2}|\mathbf{u}|^2 + Q)$ on S_{in} , $p = h_{out} - (\frac{1}{2}|\mathbf{u}|^2 + Q)$ on S_{out} , and $\partial p / \partial n = \mathbf{v} \cdot \mathbf{n} \cdot \Delta \mathbf{u}$ on S_w . With the same boundary conditions for the new reference potential ϕ as in (30), it is then easy to check that our proof of the Kelvin theorem and the JA-relation go through unchanged. However, in this alternative construction there is no guarantee that \mathbf{u}_ϕ is C^∞ at $S_{in} = S_{out}$.
- ⁴⁵L. Evans, *Partial Differential Equations*, Graduate studies in mathematics, Vol. 19 (American Mathematical Society, 2010).
- ⁴⁶O. Penttinen, E. Yasari, and H. Nilsson, "A pimpleFoam tutorial for channel flow, with respect to different LES models," *Practice Periodical on Structural Design and Construction* **23**, 1–23 (2011).
- ⁴⁷H. G. Weller, G. Tabor, H. Jasak, and C. Fureby, "A tensorial approach to computational continuum mechanics using object-oriented techniques," *Computer in Physics* **12**, 620–631 (1998).
- ⁴⁸F. Lyman, "Vorticity production at a solid boundary," *Appl. Mech. Rev.* **43**, 157–158 (1990).
- ⁴⁹R. Panton, *Incompressible Flow* (John Wiley & Sons, 1984).
- ⁵⁰B. R. Morton, "The generation and decay of vorticity," *Geophysical & Astrophysical Fluid Dynamics* **28**, 277–308 (1984).
- ⁵¹A quick way to check this is to observe that the corresponding wall-normal component of the Lamb vector, $(\mathbf{u} \times \boldsymbol{\omega})_y$, points upward, and it thus aligns with $u_{\phi y} > 0$ upstream of the bump but anti-aligns with $u_{\phi y} < 0$ downstream.
- ⁵²Y. Du and T. Zaki, "Vorticity dynamics and Josephson-Anderson relation for flow over spheroid," *Bulletin of the American Physical Society. 76th Annual Meeting of the Division of Fluid Dynamics*, Washington, DC. Session L39: Vortex Dynamics and Vortex Flows: General (2023).
- ⁵³D. Kivotides, J. Vassilicos, D. Samuels, and C. Barenghi, "Kelvin waves cascade in superfluid turbulence," *Physical review letters* **86**, 3080 (2001).
- ⁵⁴E. Kozik and B. Svistunov, "Kelvin-wave cascade and decay of superfluid turbulence," *Physical review letters* **92**, 035301 (2004).
- ⁵⁵P. Constantin and G. Iyer, "A stochastic-Lagrangian approach to the Navier–Stokes equations in domains with boundary," *Annals of Applied Probability* **21**, 1466–1492 (2011).
- ⁵⁶G. L. Eyink, A. Gupta, and T. A. Zaki, "Stochastic Lagrangian dynamics of vorticity. Part 1. General theory for viscous, incompressible fluids," *J. Fluid Mech.* **901**, A2 (2020).
- ⁵⁷G. L. Eyink, A. Gupta, and T. A. Zaki, "Stochastic Lagrangian dynamics of vorticity. Part 2. Application to near-wall channel-flow turbulence," *J. Fluid Mech.* **901**, A3 (2020).
- ⁵⁸J. Nikuradse, "Strömungsgesetze in rauhen Röhren," *VDI-Forschungsheft* 361. Beilage zu "Forschung auf dem Gebiete des Ingenieurwesens" Ausgabe B, Band 4. Translated as "Laws of flow in rough pipes," National Advisory Committee for Aeronautics, Technical Memorandum 1292, Washington, DC, 1950 (1933).
- ⁵⁹O. Cadot, Y. Couder, A. Daerr, S. Douady, and A. Tsinober, "Energy injection in closed turbulent flows: Stirring through boundary layers versus inertial stirring," *Phys. Rev. E* **56**, 427 (1997).
- ⁶⁰G. Gioia and P. Chakraborty, "Turbulent friction in rough pipes and the energy spectrum of the phenomenological theory," *Physical review letters* **96**, 044502 (2006).
- ⁶¹N. Goldenfeld, "Roughness-induced critical phenomena in a turbulent flow," *Physical review letters* **96**, 044503 (2006).
- ⁶²J. Gao, K. Agarwal, and J. Katz, "Experimental investigation of the three-dimensional flow structure around a pair of cubes immersed in the inner part of a turbulent channel flow," *J. Fluid Mech.* **918**, A31 (2021).
- ⁶³H. Quan and G. L. Eyink, "Inertial momentum dissipation for viscosity solutions of euler equations. i. flow around a smooth body," arXiv preprint arXiv:2206.05325 (2022).
- ⁶⁴S. Kumar, S. Toedtli, T. A. Zaki, and G. L. Eyink, "Josephson-Anderson relation as diagnostic of turbulent drag reduction by polymers," submitted (2024).
- ⁶⁵M. Aghaei-Jouybari, J.-H. Seo, J. Yuan, R. Mittal, and C. Meneveau, "Contributions to pressure drag in rough-wall turbulent flows: Insights from force partitioning," *Physical Review Fluids* **7**, 084602 (2022).
- ⁶⁶K. Menon and R. Mittal, "On the initiation and sustenance of flow-induced vibration of cylinders: insights from force partitioning," *Journal of Fluid Mechanics* **907**, A37 (2021).
- ⁶⁷K. Menon and R. Mittal, "Significance of the strain-dominated region around a vortex on induced aerodynamic loads," *Journal of Fluid Mechanics* **918**, R3 (2021).
- ⁶⁸K. Fukagata, K. Iwamoto, and N. Kasagi, "Contribution of Reynolds stress distribution to the skin friction in wall-bounded flows," *Physics of Fluids* **14**, L73–L76 (2002).
- ⁶⁹M. Yoon, J. Ahn, J. Hwang, and H. J. Sung, "Contribution of velocity-vorticity correlations to the frictional drag in wall-bounded turbulent flows," *Physics of Fluids* **28**, 081702 (2016).

**Supplementary Materials for “A Josephson-Anderson relation for drag in
classical channel flows with streamwise periodicity: Effects of wall
roughness”**

Samvit Kumar and Gregory L. Eyink

Department of Applied Mathematics and Statistics, Johns Hopkins University

(*skumar67@jh.edu, eyink@jhu.edu)

(Dated: July 2, 2024)

arXiv:2407.01416v1 [physics.flu-dyn] 1 Jul 2024

CONTENTS

I. Huggins' Reference Potential Flow	3
II. Velocity and Vorticity Fields at Drag Maximum & Minimum	4
III. JA Transfer Integrands At Drag Maximum & Minimum	5
IV. Pressure Fields	6

I. HUGGINS' REFERENCE POTENTIAL FLOW

The Fig.3 in the main text plotted the wall-normal components of Huggin's reference potential flow velocity at the inflow and outflow cross-sections. Here we plot the other two velocity components.

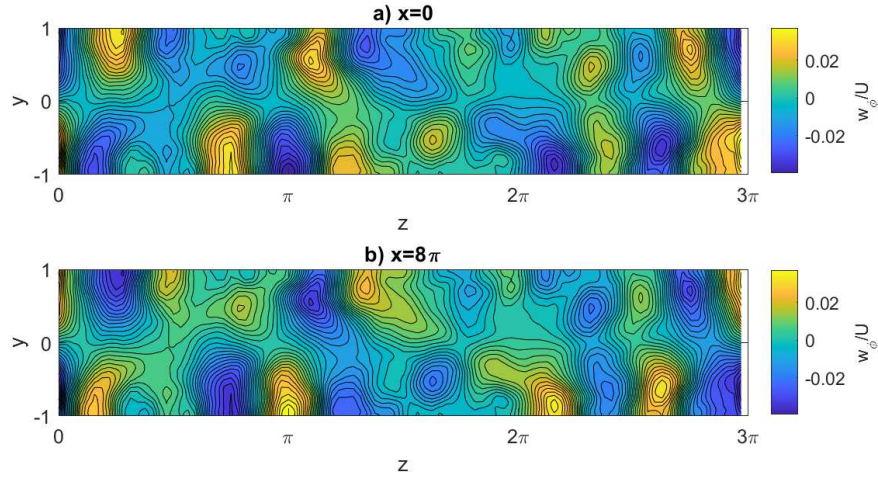


FIG. 1: Anti-periodic spanwise component of Huggins' potential flow velocity for a flat-wall turbulent channel flow, at inflow $x = 0$ and outflow $x = 8\pi$.

The above plot of the spanwise component of Huggin's reference potential velocity shows that it, like the wall-normal component, is streamwise anti-periodic.

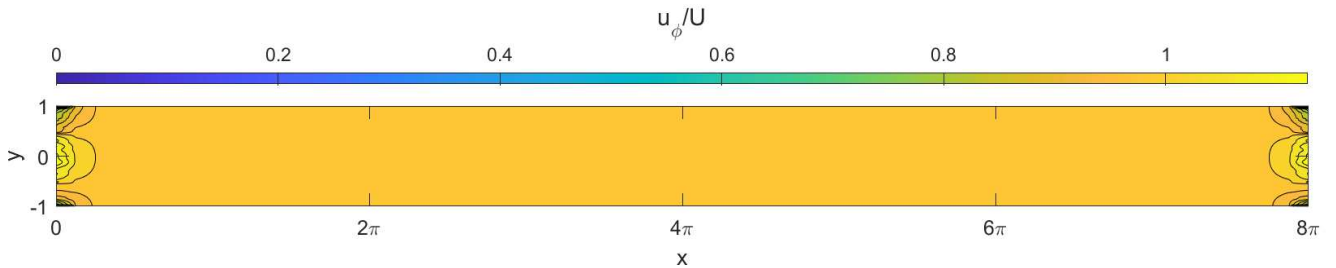


FIG. 2: Periodic streamwise component of Huggins' potential flow velocity for a flat-wall turbulent channel flow, in the spanwise midplane $z = 3\pi/2$.

The streamwise component of the reference potential velocity in Huggin's construction is guaranteed to be periodic, as verified in the above plot. Inertial adjustment toward plug flow away from inflow/outflow is observed, just as in the plot of the streamlines in Fig. 2a of the main text.

II. VELOCITY AND VORTICITY FIELDS AT DRAG MAXIMUM & MINIMUM

Plotted here are the same fields in the same flow sections as appear in Fig. 8 of the main text for the time $tU/L_x = 9.75$, but now at times of local maximum and minimum drag.



FIG. 3: Instantaneous (a) wall-normal velocity, normalized by U , and (b) spanwise vorticity field normalized by U/L_x , at spanwise plane $z = 0.25$ and time $tU/L_x = 3.51$ of local maximum drag



FIG. 4: Instantaneous (a) wall-normal velocity, normalized by U , and (b) spanwise vorticity field normalized by U/L_x , at spanwise plane $z = 0.25$ and time $tU/L_x = 4.485$ of local minimum drag

The main features which are apparent at the time of local maximum drag are the larger wall-normal velocities and also the more intense negative spanwise vorticity on the upstream side of the bump. Note that the point of separation on the downstream side is almost the same at both times.

III. JA TRANSFER INTEGRANDS AT DRAG MAXIMUM & MINIMUM

Plotted here are the same fields in the same flow sections as appear in Fig. 9 of the main text for the time $tU/L_x = 9.75$, but now at times of local maximum and minimum drag.

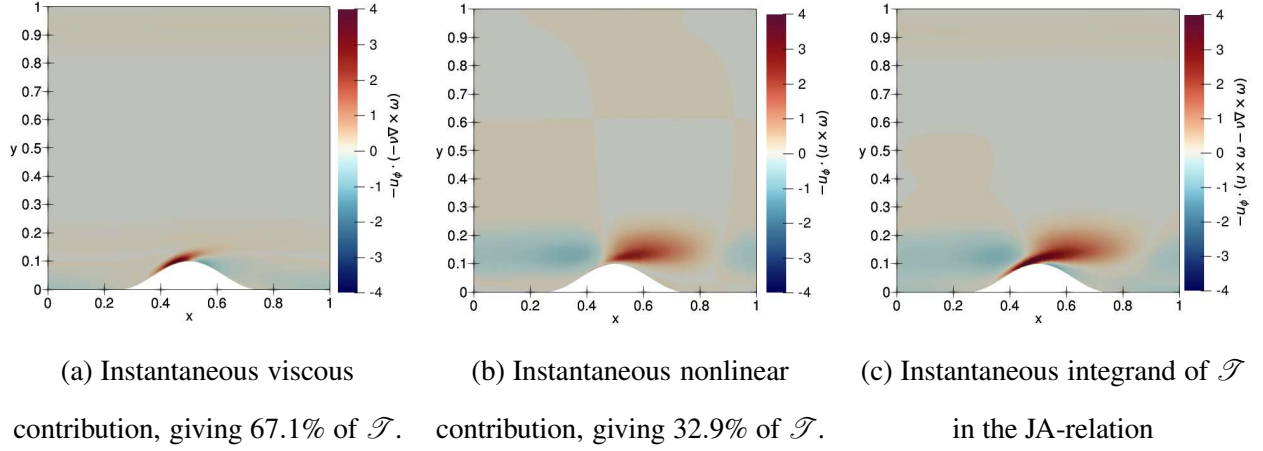


FIG. 5: Instantaneous fields of (a) the integrand of \mathcal{T} , (b) viscous and (c) nonlinear contributions to the integrand, all normalized by $\rho U^3/L_x$. Fields are shown at spanwise plane $z = 0.25$ and time $tU/L_x = 3.51$ of local maximum drag

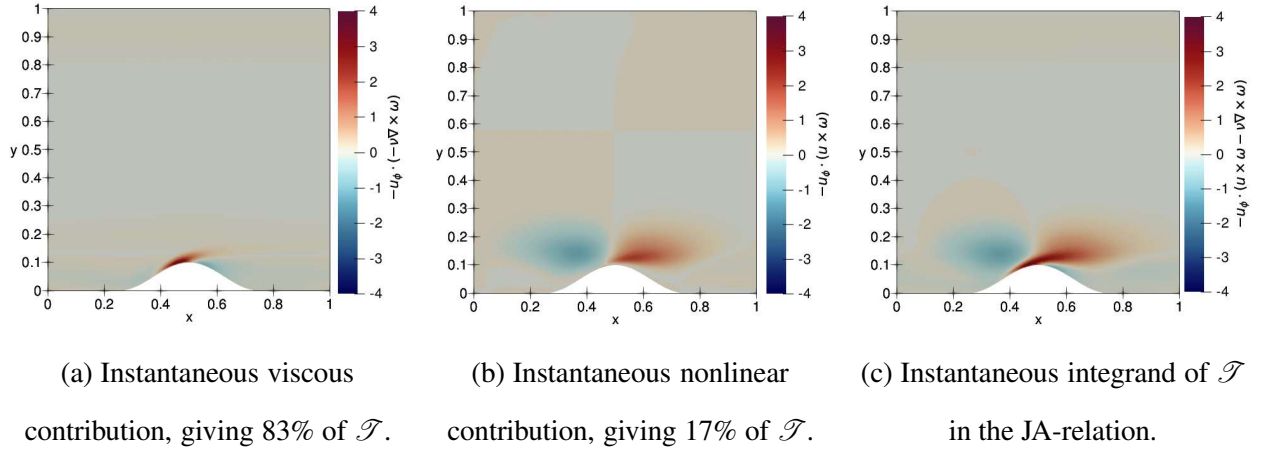


FIG. 6: Instantaneous fields of (a) the integrand of \mathcal{T} , (b) viscous and (c) nonlinear contributions to the integrand, all normalized by $\rho U^3/L_x$. Fields are shown at spanwise plane $z = 0.25$ and time $tU/L_x = 4.485$ of local minimum drag

A main result is the stronger contribution from vortex shedding at the time of local maximum drag. Also notable is a somewhat stronger "anti-drag" lobe upstream at the time of local minimum drag.

IV. PRESSURE FIELDS

We show here the pressure fields at several key instants in our flow.

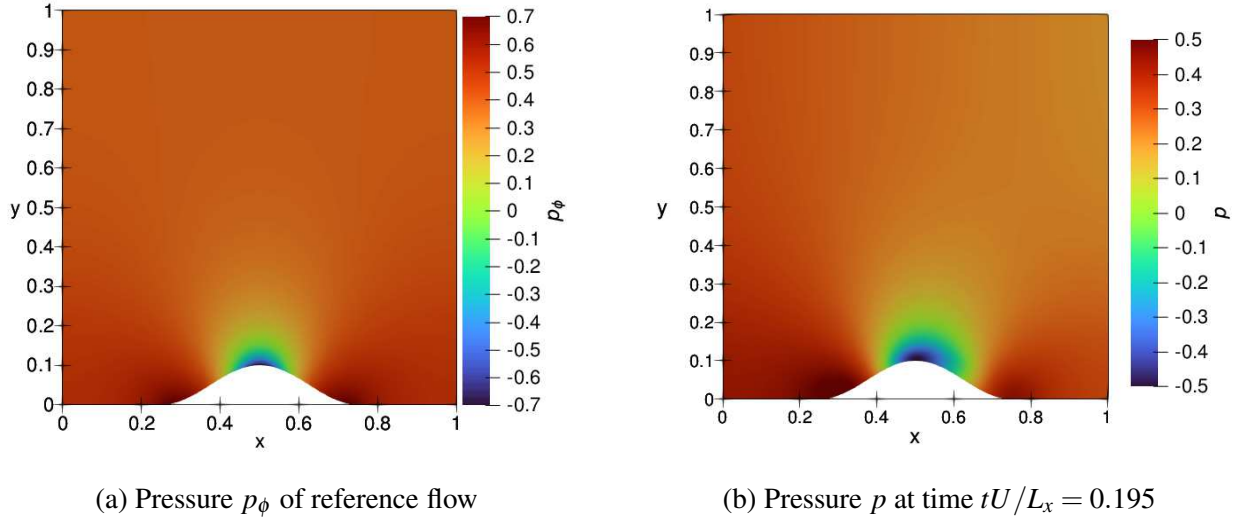


FIG. 7: Pressure of the background potential Euler flow and pressure at an early time

The pressure p_ϕ of our new reference potential Euler solution can be calculated from the Bernoulli relation, $p_\phi + (1/2)\rho|\mathbf{u}_\phi|^2 = c(t)$. For the flow over the bump described in the main text of the paper, the associated potential pressure field is shown in Fig. 7a. Naturally, there is no form drag for the current case, where the bulk velocity U is constant in time, and the potential pressure is perfectly symmetric about $x = 0.5$. The Navier-Stokes flow discussed in the main text is initialized with plug flow, which is close to \mathbf{u}_ϕ , and the pressure p from the Poisson equation at early times is close to p_ϕ , as illustrated in Fig. 7b for time $tU/L_x = 0.195$. However, a slight asymmetry has developed in p due to rotational pressure p_ω , which results in some form drag.

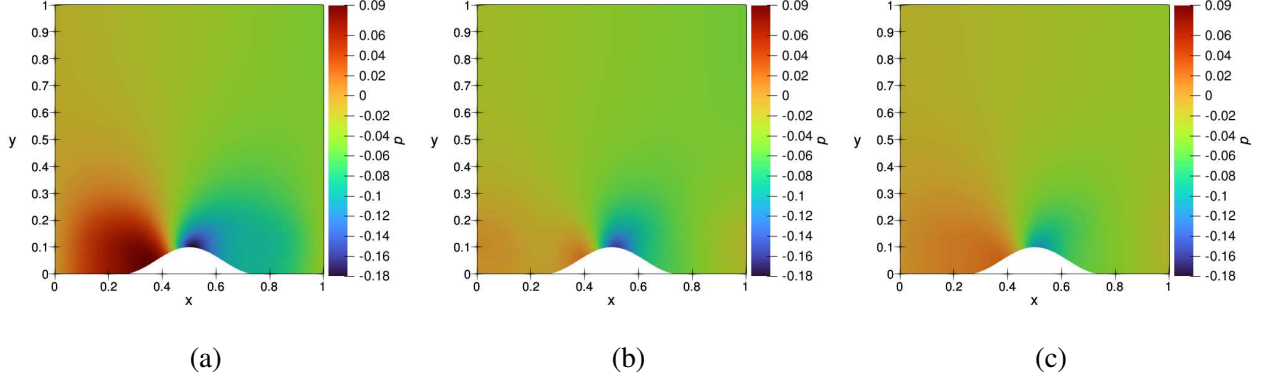


FIG. 8: Instantaneous pressure fields at $z=0.25$ for (a) $tU/L_x = 3.51$, (b) $tU/L_x = 4.485$ (c) $tU/L_x = 9.75$, all normalized by ρU^2 .

We show instantaneous pressure fields at a time of local maximum drag ($tU/L_x = 3.51$) in Fig. 8a, at a time of local minimum drag ($tU/L_x = 4.458$) in Fig. 8b, and at the late time $tU/L_x = 9.75$ discussed in detail in the main text in Fig. 8c. The pressure difference on the upstream and downstream faces of the bump is much higher for the local drag maximum when compared with the other two instants. This is consistent by Lighthill's relation $\sigma = -\mathbf{n} \times \nabla p$ with the greater magnitude of negative spanwise vorticity shed into the flow in this case, as observed in Fig. 3b. Notice that the pressure magnitudes have dropped significantly at all of these times compared to the potential pressure p_ϕ and the pressure p at the early time $tU/L_x = 0.195$ presented in Fig. 7.